Sustainable Food Technology

ROYAL SOCIETY OF CHEMISTRY

PAPER

View Article Online
View Journal

Cite this: DOI: 10.1039/d5fb00744e

Prolonging fruit shelf-life with a graphitic carbon nitride (GCN) incorporating biopolymer composite: layer-by-layer assembled coating

Md. Sajib Hossain,[a] Md. Didarul Islam,[b] Anik Das,[c] M. Mehedi Hasan,[d] Md. Mahfuzur Rahman[e] and Samrat Mukhopadhyay *[a]

This study presents a novel, biodegradable, and multifunctional layer-by-layer (LbL) coating composed of sodium alginate (SA), chitosan (CAS), and graphitic carbon nitride (GCN) for efficient fruit preservation. The integration of GCN into the SA/CAS matrix significantly enhanced UV shielding, antimicrobial activity, and ethylene scavenging, while maintaining excellent biocompatibility and minimal leaching of GCN. The LbL-coated fruits demonstrated extended shelf life of 15 days for grapes and 10 days for bananas, outperforming uncoated controls. The coating has superior thermal stability, reduced swelling, low moisture permeability, and strong adhesion on irregular fruit surfaces. Importantly, the synergistic action of CAS and GCN delivered over 97% bacterial inhibition, while maintaining cell viability above 90%. These findings establish SA/GCN/CAS/GCN coatings as a safe, scalable, and sustainable alternative to plastic-based packaging. In essence, this is the first report of a GCN-based LbL edible coating that combines biodegradability, antimicrobial performance, UV protection, and fruit shelf-life extension, offering a green solution for modern food packaging challenges.

Received 6th November 2025
Accepted 7th January 2026

DOI: 10.1039/d5fb00744e

rsc.li/susfoodtech

Sustainability spotlight

This study advances sustainable food packaging through a biodegradable, edible composite film made from chitosan, alginate, and graphitic carbon nitride (g-C_3N_4). By extracting chitosan from waste shrimp shells and using non-toxic, water-based processing, the work upcycles marine waste into high-value materials. The coating enhances UV blocking, antimicrobial activity, and water-vapor resistance, extending fruit shelf life by over 100% while replacing single-use plastics. This innovation supports the UN Sustainable Development Goals: SDG 2 (Zero Hunger) by reducing food loss, SDG 3 (Good Health and Well-Being) through non-toxic materials, SDG 12 (Responsible Consumption and Production) *via* waste valorization and SDG 13 (Climate Action) by reducing plastic pollution. It represents a circular, eco-friendly path toward sustainable food preservation.

1. Introduction

The worldwide struggle to secure food supplies is exacerbated by large post-harvest losses in easily perishable fruits and vegetables, of which 45% are lost each year due to rapid spoilage losses that are largely due to microbiological contamination, moisture loss and ethylene-induced ripening, which compromise the quality, safety and marketability of fresh produce. With an increasing global population and an increasing demand for food, there is an urgent need to increase the shelf life of perishable foodstuffs with safe, cost-effective, and environmentally friendly packaging.[1–3]

Edible coatings/films are being increasingly used as an alternative or auxiliary method for post-harvest preservation. Unlike common plastic packaging, these edible coatings provide the possibility of being biodegradable, biocompatible, and safe for direct contact with food, which can solve both the environmental and food safety issues.[2,4] Among the candidates, polysaccharide-based coatings, in particular, sodium alginate (SA) and chitosan (CAS), are promising due to their film-forming nature, low toxicity, and functional capability.[5–7]

Natural anionic polysaccharide sodium alginate, derived from brown seaweed, constitutes a water-soluble and flexible hydrophilic film with excellent oxygen barrier performance and has been used at food levels.[8,9] Alginate is cross-linked with multivalent ions such as Ca^{2+} and Zn^{2+}, endowing increased mechanical stability. However, the antimicrobial activity of SA based coatings alone is relatively low, and the air permeability is poor, leading to unsatisfactory effects in inhibiting spoilage.[10–12]

[a]Indian Institute of Technology, Hauz Khas, New Delhi-110016, India. E-mail: samrat@textile.iitd.ac.in&rdquo
[b]Department of Applied Chemistry and Chemical Engineering, Noakhali Science and Technology University (NSTU), Noakhali-3814, Bangladesh
[c]National Institute of Textile Engineering and Research, University of Dhaka, Dhaka 1000, Bangladesh
[d]Department of Chemistry, Virginia Tech, Blacksburg, Virginia 24061, USA
[e]Industrial and Production Engineering, Jashore University of Science and Technology (JUST), Jashore, Bangladesh

These weaknesses can be overcome by adding SA with chitosan (CAS) (a cationic polysaccharide), which possesses antimicrobial and broad-spectrum antioxidant characteristics.[13–15] The reactive amine groups of CAS can easily be ionically crosslinked with SA to produce well-defined polyelectrolyte complexes (PECs), which greatly enhance the mechanical strength, gas barrier properties, and antimicrobial activities of the resultant composite films.[16–18]

However, traditional mixing of SA and CHT generally results in the non-uniformity of coatings, which makes the coatings less effective on the irregular surfaces of fruit. LbL assembly represents an attractive alternative as it enables precise deposition of oppositely charged polyelectrolyte layers and the formation of LbL coatings,[19–22] where their composition can be fine-tuned to obtain uniform coatings with the desired properties.[23] In these types of film fabrication processes, multilayered film structures are formed, which can be widely applied to various substances and polymeric materials.[24,25]

Nonetheless, even LbL coatings fail to actively reduce ethylene accumulation or UV-induced oxidative damage, which contributes to the enhancement of ripening and microorganism growth, respectively. The incorporation of functional nanomaterials in a biopolymer framework has been presented as a promising way forward. In recent times, graphene-like carbon nitrides (GCNs) have been increasingly used as a next-generation additive in food packaging. The metal-free, organic semiconductor GCN has exhibited great photocatalytic activity, chemical stability, and biocompatibility.[15] The produced hydroxyl reactive species radicals and superoxide anion (ROS) by GCN under visible light possess strong "*in vitro*" antimicrobial activities against several typical food-borne pathogens such as *E. coli*, *Salmonella*, and *Listeria*.[15,26] Moreover, GCN can act as a catalyst for the photodecomposition of ethylene gas, a natural ripening agent, potentially leading to the inhibition of the softening of fruits and the occurrence of senescence. A 2D layered stacked structure also enhances mechanical reinforcement and UV shielding, which is beneficial in extending the shelf life of food.[27,28] Although these features are very promising, the application of GCN in the field of food coatings is, to a large extent, unexplored. A versatile biodegradable LbL coating using SA, CAS, and GCN was constructed by electrostatic self-assembly. GCN as an active nanofiller was embedded between the negatively charged SA and the positively charged CAS layers. The application of this layered system is proposed to take advantage of the synergistic effects of the three components: the film-forming and gas barrier effects of SA, the antibacterial properties of CAS, and ethylene absorbing and UV-blocking capacities of GCN.[29,30] The present study successfully developed a new biodegradable LbL coating composed of SA, CAS, and GCN using a LbL method, which examines physicochemical, structural, antimicrobial, and preservation properties of SA, CAS and GCN composite coatings fabricated based on LbL self-assembly on fresh fruits. Morphological, compositional, and textural characteristics were evaluated with SEM, FTIR, TGA, XRD, TEM, and BET. Important functional properties, such as the swelling index (SI), water vapour permeability (WVP), UV blocking, antimicrobial activity, and GCN release behaviour, were studied. The coating efficacy was also confirmed by shelf-life extension tests on fresh grapes and bananas. To the best of our knowledge, this is the first study using GCN in an LbL coating for food preservation. This study proposes a new green strategy for post-harvest protection based on biopolymers and a biocompatible photocatalyst and could be adapted to be a sustainable alternative to synthetic preservatives and non-degradable packaging.

2. Experiential section

2.1. Materials

Sodium alginate ($M_w = 3.0 \times 10^5$ g mol^{-1}) was purchased from Loba Chemie Pvt., Ltd. Sodium hydroxide (NaOH, 99%), hydrochloric acid (HCl, 37%), and glacial acetic acid (CH_3-COOH, 100%) were procured from Merck, Germany. Urea ($CO(NH_2)_2$, 99%) and nitric acid (HNO_3, 60%) were procured from Merck, India. L929 mouse fibroblast cells were procured from Centyle Biotech Private Limited, India. Distilled water (DI) was used throughout the experiments. All chemicals used in the experiment were of analytical grade.

2.2 Methods

2.2.1. Synthesis of GCN. Graphitic carbon nitride (GCN) was synthesized by thermally decomposing anhydrous urea, following a procedure similar to that outlined by Cui *et al.*[31] Initially, 5 g of urea was placed in a 100 mL porcelain crucible and dried in an oven at 90 °C for 12 hours under ambient pressure. The crucible was then transferred to a muffle furnace,

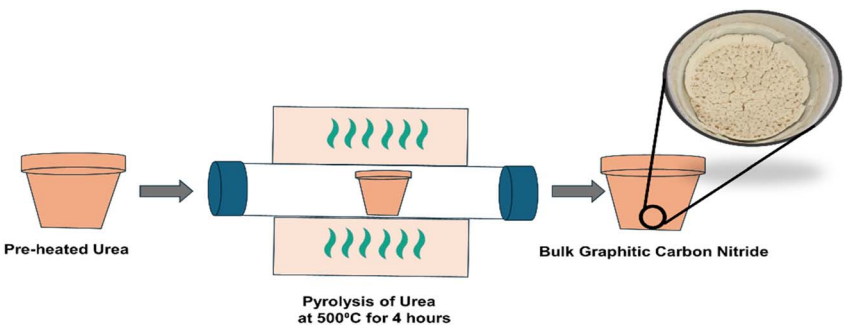

Fig. 1 Schematic diagram of the graphitic carbon nitride synthesis process.

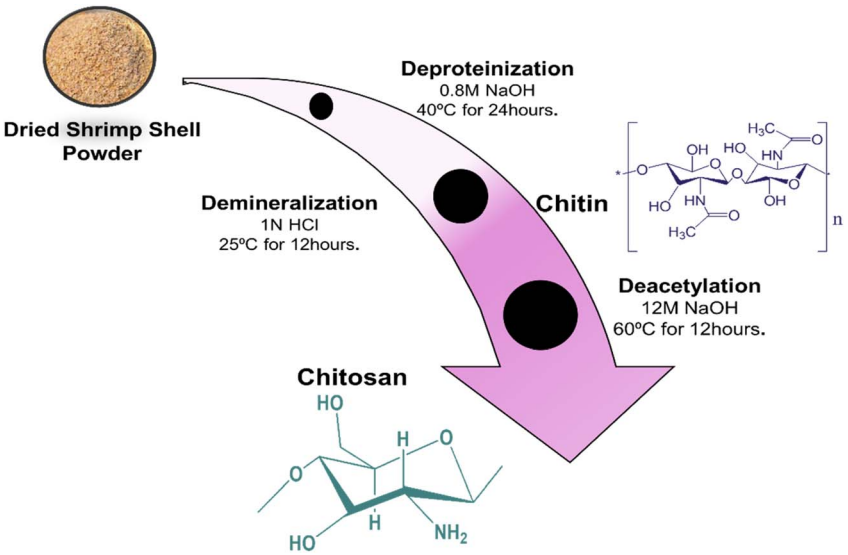

Fig. 2 Schematic diagram of the chitosan synthesis process.

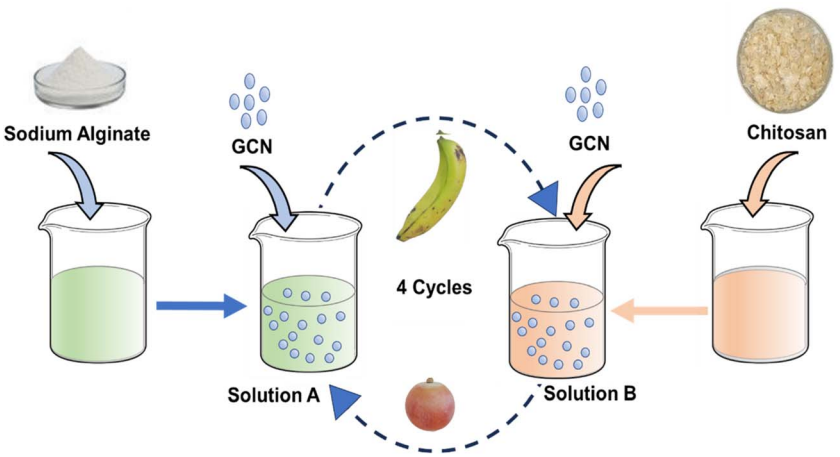

Fig. 3 Systematic representation of layer-by-layer assembly.

where the temperature was gradually increased from 25 °C to 500 °C at a heating rate of 10 °C per minute. Once the furnace reached 500 °C, the sample was held at this temperature for 4 hours to allow for polymerization. After the reaction, the sample was allowed to cool slowly to room temperature. To remove any alkaline residues, the product was washed with a 0.1 mol L^{-1} nitric acid solution, followed by multiple rinses with deionized water. Finally, the GCN product was dried at 95 °C for 3 hours to obtain the desired powder (Fig. 1).

2.2.2. Synthesis of chitosan (CAS). Over the past few decades, numerous approaches have been developed for extracting CAS from prawn shells.[32–35] Initially, the prawn shells were thoroughly washed, dried, and then ground into smaller pieces. The crushed shells were subjected to deproteinization by treatment with 0.80 M NaOH at 40 °C for 24 hours, effectively removing the protein content. Following this, the alkali-insoluble material was rinsed with deionized water until the pH reached neutral. The protein-free shells were then demineralized using 1N HCl for 12 hours, with continuous stirring at ambient temperature. After demineralization, the shrimp shells were processed into chitin. The resulting chitin was deacetylated by heating it with 12 M NaOH at 60 °C for 12 hours. Once the deacetylation process was completed, the sample was thoroughly washed until a neutral pH was achieved. Finally, the obtained CAS fraction was dried (Fig. 2).

2.2.3. Preparation of SA/GCN/CAS/GCN LbL coating. To prepare a thin layer-by-layer coating on the fruit's surface, a uniform dispersed solution of SA/GCN and CAS/GCN was initially prepared, as shown in Fig. 3. For the SA/GCN dispersed solution preparation, 2 g SA was dissolved in 80 ml of DI water, which was mixed with 20 ml of a dispersed (by sonication) GCN solution (2 g L^{-1}). This solution is referred to as "Solution A."

For the CAS/GCN dispersed solution preparation, 0.5 g of CAS was dissolved in an 80 ml 0.35 M acetic acid solution by continuous stirring. Following complete dissolution, 20 mL of a sonication-dispersed GCN solution (2 g L^{-1}) was introduced to adjust the pH to 6.1. This preparation is hereafter denoted as

Solution B. All film-forming solutions were kept under ambient conditions for 2 hours for complete degasification.

To prepare the intercalated fourth-layer food coating (LbL coating), fruit samples were first immersed in Solution A for 20 s, followed by removal of excess solution for 2 min. The samples were then immersed in Solution B for 20 s to deposit a CAS/GCN film over the SA/GCN film, after which the excess solution was again removed for 2 min. Subsequently, the coated fruits were dried at room temperature for 20 min under continuous airflow by suspending them on a stand. This complete sequence was considered as one coating layer. This process was continued four times (4 layers) to produce an intercalated triple-layered fruit coating layer and obtain the SA/GCN/CAS/GCN layer by layer coating.

3. Characterization techniques

X-ray diffraction (XRD) analysis was performed using an Ultima IV diffractometer (Rigaku, Japan) with Cu Kα radiation (λ = 1.5406 Å) to determine the crystal structure and phase composition of GCN. Scans were collected over a 2θ range of 10–60° at 4° min^{-1} with a step size of 0.04°. Fourier transform infrared (FTIR) spectra were obtained using a Nicolet 6700 spectrometer (Thermo Fisher, USA) in ATR mode within 500–4000 cm^{-1} (resolution = 4 cm^{-1}) to identify functional groups and chemical interactions. Thermogravimetric analysis (TGA) was conducted on a PerkinElmer TGA 4000 (USA) from room temperature to 800 °C at 10 °C min^{-1} under nitrogen flow (20 mL min^{-1}) to assess thermal stability and composition. Morphological features were examined using a ZEISS Sigma 300 SEM after gold sputtering, and elemental distribution was determined by EDX spectroscopy. Specific surface area and porosity were analyzed by the Brunauer–Emmett–Teller (BET) method using a Nova 800 analyzer (Anton Paar, USA) after degassing at 150 °C for 12 h. High-resolution TEM images were recorded on a Tecnai™ G2 20 (FEI, USA) operating at 200 kV. Samples were ultrasonically dispersed in ethanol and drop-cast onto carbon-coated copper grids before observation.

3.1 UV and (high energy blue light) HEBL shielding effectiveness

The UV and HEBL shielding effectiveness of the samples was examined by measuring the optical transmittance in the 200–500 nm wavelength range using UV-vis (Shimadzu UV-2600) spectrophotometers with an integrating sphere. All experiments were performed at room temperature under ambient conditions. Thin films were prepared on quartz substrates. The transmittance was measured at UVA (315–400 nm) and UVB (280–315 nm) for UV absorbent analysis. The percentage of UV blocking was determined according to the following formula:

$$\text{UV blocking efficiency } (\%) = \left(1 - \frac{T_{UV}}{T_{ref}}\right) \times 100 \quad (1)$$

where T_{UV} is the transmittance of the sample in the UV range and T_{ref} is the transmittance of the bare quartz substrate.

3.2 Leaching analysis of nanofillers

The U.S. Environmental Protection Agency (EPA 111) (Toxicity Characteristic Leaching Procedure) TCLP was employed to discover how nanofillers were released from the coating specimens. The leaching medium was composed of phosphate-buffered saline (PBS) at 5 °C, where the samples were incubated and stirred at 300 rpm for 300 minutes. At specific time points (15, 30, 60, 120, 180, 240, and 300 minutes), small samples of the leaching solution were taken and analyzed with UV-vis spectroscopy to measure how many nanoparticles had been released. The concentration of released nanofillers at the above time intervals (C_t, mg L^{-1}) was quantified, and the cumulative release (R_t) was calculated according to the following equation:

$$R_t = \frac{C_t V}{m} \quad (2)$$

Here, C_t is the concentration of nanofillers in the leaching solution at time t, V is the volume of the solution in liters, and M is the original mass of nanofillers in the sample. The total percentage of nanofillers released (%L) was then calculated using these values:

$$\%\ L = \left(\frac{M_t}{M_o}\right) \times 100 \quad (3)$$

3.3 Swelling index (SI) measurement

The swelling behavior of the samples was tested by placing them in phosphate-buffered saline (PBS) at 30 °C for 2 hours. Dry samples were weighed first (W_d) and then immersed in PBS. At specific time intervals, the samples were taken out, gently blotted with filter paper to remove surface water, and weighed again (W_s). The swelling index (%SI) was calculated from the weight increase, which shows how much water the samples absorbed:

$$\%\ \text{SI} = \frac{W_s - W_d}{W_d} \times 100 \quad (4)$$

3.4 Moisture content determination

The moisture content (%MC) of the samples was measured using a gravimetric method. Each sample was first weighed (W_i) and then dried in an oven at 110 °C until its weight stopped changing (W_f). The moisture content was calculated using the weight difference, which shows how much water was present in the sample:

$$\%\ \text{MC} = \frac{W_i - W_f}{W_i} \times 100 \quad (5)$$

3.5 Water solubility (WS) test

The water solubility of the samples was measured using a gravimetric method. Dry specimens (0.2 g) were weighed and then soaked in 50 mL of distilled water in sealed glass containers at room temperature (25 ± 1 °C) for 24 hours without stirring. After soaking, the undissolved material was collected by filtration, gently rinsed with distilled water to remove any surface residues, and dried at 60 °C until the weight became constant (W_f). The

water solubility was then calculated using the following equation, which shows how much of the sample dissolved in water.

$$\mathrm{WS} = \frac{W_i - W_f}{W_i} \times 100 \quad (6)$$

3.6 Water contact angle (WCA)

The wettability of the sample surfaces was tested by measuring the static water contact angle (WCA) using a contact angle goniometer (Krüss DSA30, Germany). A 3 μL droplet of deionized water was carefully placed on the surface using an automated system (sessile drop method). All measurements were done at room temperature (22 ± 1 °C). Photos of the water droplet were taken immediately, and the contact angle was calculated using the goniometer built-in image analysis software (ADVANCE, Krüss), which shows how easily water spreads on the surface.

3.7 Antimicrobial assay

Microbial growth and reproduction are the main causes of food spoilage and quality loss. Therefore, testing the antimicrobial properties is an important part of evaluating food packaging materials. In this study, the antimicrobial activity of three film compositions SA, SA/GCN, and SA/GCN/CAS/GCN was tested against Gram-negative *Escherichia coli* (*E. coli*) and Gram-positive *Staphylococcus aureus* (*S. aureus*). Bacterial suspensions were first grown in the Luria Broth (LB) nutrient medium overnight until they reached an optical density of 0.08–0.10 at 600 nm, verified with a UV-vis spectrophotometer. The suspension was then serially diluted five times, with each tube containing 9 mL of distilled water, resulting in a cell concentration of 2.7×10^8 CFU per mL. Antimicrobial activity was tested using both the colony-forming unit (CFU) method and the disk diffusion method, following AATCC 100-2004 test standards.

3.7.1. Disk diffusion assay. At the start of the experiment, nutrient agar plates were prepared and inoculated with 1 mL each of *Escherichia coli* (*E. coli*) and *Staphylococcus aureus* (*S. aureus*) using a spreader. Three circular specimens, each 5 mm in diameter, were then placed onto the agar. The plates were incubated at 37 °C for 24 hours. After incubation, the plates were photographed, and the size of the antibacterial zone of inhibition was measured using Image J software, with results expressed in area units. To ensure accuracy, each film was tested at least three times.

3.7.2. Colony forming unit (CFU) assay. 1-inch by 1-inch coated film samples were placed in test tubes with 10 mL of distilled water and sterilized by autoclaving. The tubes were then exposed to UV light for 30 minutes. After that, 0.1 mL of bacterial suspension (2.7×10^9 CFU per mL) was added to each tube, and the tubes were incubated at 37 °C for 24 hours. The next day, a four-fold serial dilution was performed, and 0.1 mL of each diluted sample was spread onto agar plates. The plates were incubated at 37 °C for another 24 hours, and on the third day, bacterial colonies were counted and calculated using the appropriate formula:

$$\text{Kill efficiency } (\%) = \frac{B - A}{B} \times 100 \quad (7)$$

A: survivor cell count of the treated sample and B: cell count of the control sample

$$\mathrm{CFU(per\ mL)} = \frac{\text{bacterial cell count on plate}}{\text{dilution factor} \times \text{volume of culture plate}} \quad (8)$$

3.8 "*In vitro*" cytotoxicity study

Cytotoxicity on L929 (Centyle Biotech Private Limited, India) mouse fibroblast cells was tested using the MTT cell viability method. L929 cells were seeded in a 96-well plate at 1×10^4 cells per well in an MEM medium containing 10% fetal bovine serum (FBS) and 1% L-glutamine. The plate was incubated at 37 °C with 5% CO_2 for 24 hours. Then, the cells were treated with different concentrations of the test solution (25, 50, 100, and 200 mg mL^{-1}) for another 24 hours. After treatment, the medium was replaced with a fresh medium containing 10% MTT solution, and the plates were incubated in the dark for 3 hours. The MTT solution was removed, and 100 μL of DMSO was added to dissolve the formazan crystals formed by living cells. The plates were gently shaken for 15 minutes, and absorbance was measured at 570 nm. Hydrogen peroxide (500 μM or 17 mg L^{-1}) was used as a positive control, while phosphate-buffered saline served as a negative control.

Percentage cell viability (%) was calculated as follows

$$\text{Cell viability} = \frac{\text{experimental absorbance} - \text{background absorbance}}{\text{PBS control for materials absorbance background absorbance}} \times 100 \quad (9)$$

3.9 Soil burial test

The biodegradability of the samples was tested using a soil burial method in the lab. Small rectangular pieces (2 cm × 2 cm) were weighed (initial dry weight, W_0) and buried about 5 cm deep in natural garden soil inside plastic containers. The soil was kept moist at 60% of its water-holding capacity and maintained at room temperature (25 ± 2 °C). Samples were taken out at 5, 10, 15, 20, 25, and 30 days, gently washed to remove soil, dried at 60 °C until their weight was constant, and weighed again (final dry weight, W_t). The percentage of weight loss was then calculated using the formula:

$$\text{Weight loss} = \frac{W_o - W_t}{W_o} \times 100 \quad (10)$$

4. Results and discussion

4.1. Characterization of GCN

Fig. 4a shows the EDX spectra, and Fig. 4b shows the GCN particles. EDX analysis indicates that GCN contains 38.21% carbon, 55.10% nitrogen, and 6.69% oxygen. The C/N atomic ratio is 0.70, which is slightly lower than the theoretical value of 0.75. This lower ratio may be due to incomplete crystallization or the presence of defect sites caused by a low degree of polymerization.[36] The 6.69% oxygen shows that water is adsorbed on the surface of GCN.[37] The SEM image in Fig. 4c shows that the synthesized GCN forms micrometer-sized particles. GCN has a porous structure, as confirmed by the N_2 adsorption–

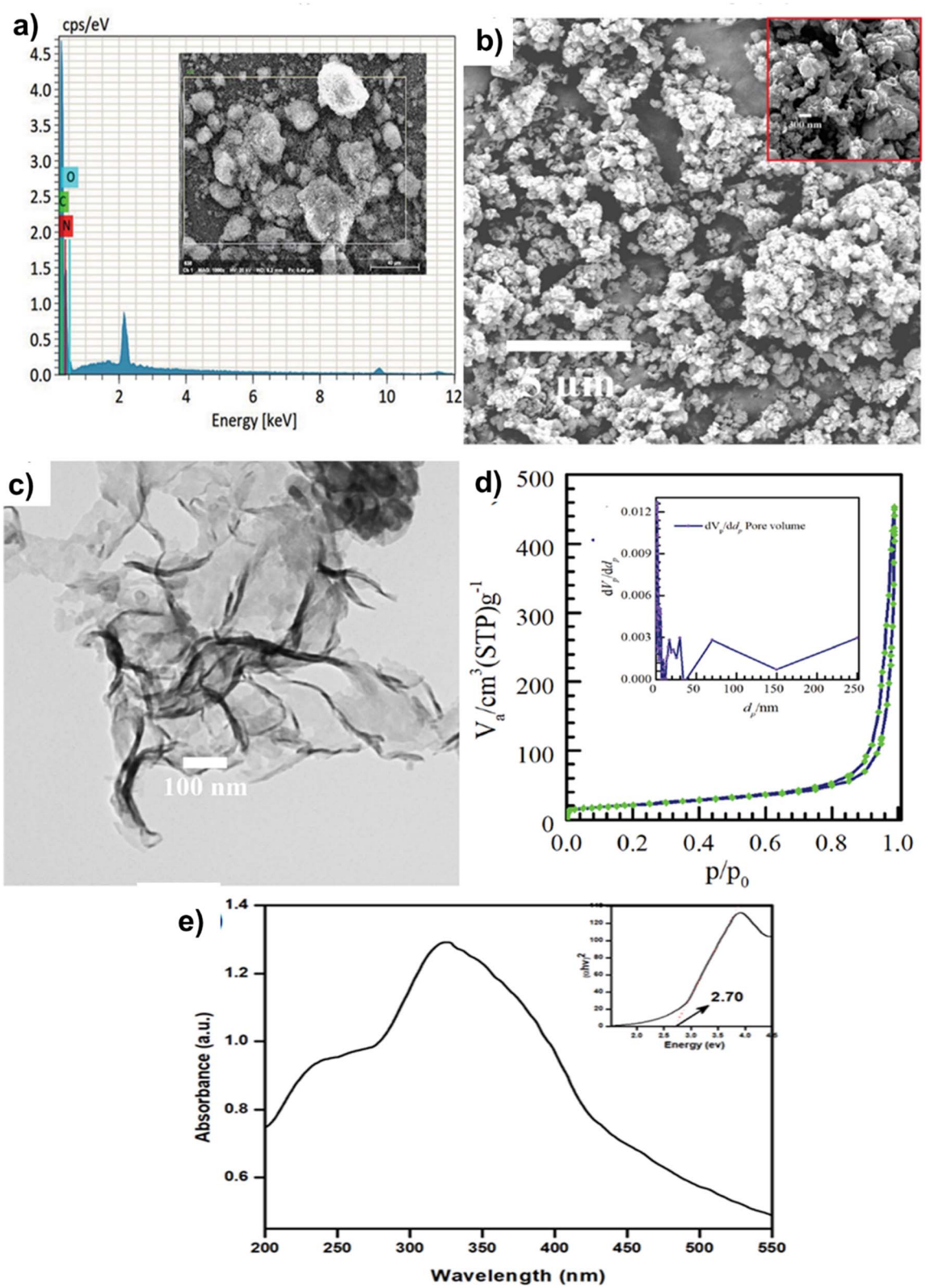

Fig. 4 Structural characterisation of graphitic carbon nitride (GCN). (a) EDX spectra of the GCN particles; (b) morphology and size distribution of GCN particles; (c) transmission electron microscope image of the 2D planar structure of GCN; (d) BET N_2 adsorption–desorption isotherm of GCN; and (e)UV-vis absorption peak of GCN.

desorption isotherm (Fig. 4d). Its surface area is about 73.6 m^2 g^{-1}, and the average pore diameter is around 35.6 nm (Fig. 4d inset). This porous structure can influence water vapor permeability in the composite film by providing extra pathways for vapor to pass through. Additionally, the high surface area of GCN increases the number of active sites for adsorbing reactants, which enhances the film's photocatalytic and antimicrobial performance.

The optical properties of the dispersed GCN were measured using UV-vis diffuse reflectance spectroscopy (Fig. 4e). A strong absorption peak appears at around 330 nm, with a smaller shoulder near 240 nm in the UV region. The band gap energy, determined from the Tauc plot (Fig. 4e inset), is 2.70 eV.[38,39] The bands at 240 nm and 330 nm are due to π–π or n–π electronic transitions within the carbon and nitrogen atoms.[39,40] The absorption peak at 330 nm, in the visible range, is mainly caused by the movement of free electrons in the GCN units within the 2D nanosheets along the planar direction.[39] The broad absorption of GCN in the visible range is likely due to defects in its crystal structure. These defects create localized sites that can trap electrons and holes, which increases the material's ability to absorb light.[41] In addition, the Tauc plot shows a band gap of 2.70 eV, which means the prepared GCN can effectively absorb UV light from sunlight.

4.2 Fourier-transform infrared (FTIR)

Fig. 5a shows the FTIR spectra of (a) GCN, (b) SA, (c) CAS, and (d) the SA/GCN/CAS/GCN layer-by-layer coating in the 4000–500 cm^{-1} range. For GCN (Fig. 5a), several peaks between 1220 and 1630 cm^{-1} confirm the presence of heterocyclic rings: peaks at 1219, 1304, and 1404 cm^{-1} correspond to C–N stretching, while peaks at 1552 and 1622 cm^{-1} are attributed to C=N stretching in the aromatic framework. The broad absorption band observed in the range of 3200–3600 cm^{-1} arises from N–H stretching vibrations of surface amine groups and O–H stretching of adsorbed water molecules, indicating hydrogen bonding and defect sites. Weak bands at around 2900 cm^{-1} are assigned to aliphatic C–H stretching vibrations. The characteristic peak at 805 cm^{-1} originates from the breathing mode of the heptazine ring units.[42–44] The broad absorption band in the range of 3200–3600 cm^{-1} is attributed to N–H stretching vibrations from surface amine groups and O–H stretching of adsorbed water molecules. The weak bands at around 2900 cm^{-1} correspond to aliphatic C–H stretching vibrations[37,39] The peaks at 1219 and 1304 cm^{-1} show that C–N bonds are present in the structure.[42,45] The broad peak also shows that there are defect sites and that hydrogen bonds form between the amine groups.[39,42,43] Also, the peak at 805 cm^{-1} comes from the vibrations of the heptazine rings.[39] The SA spectrum (Fig. (5a and b)) shows a broad peak at 3387 cm^{-1}

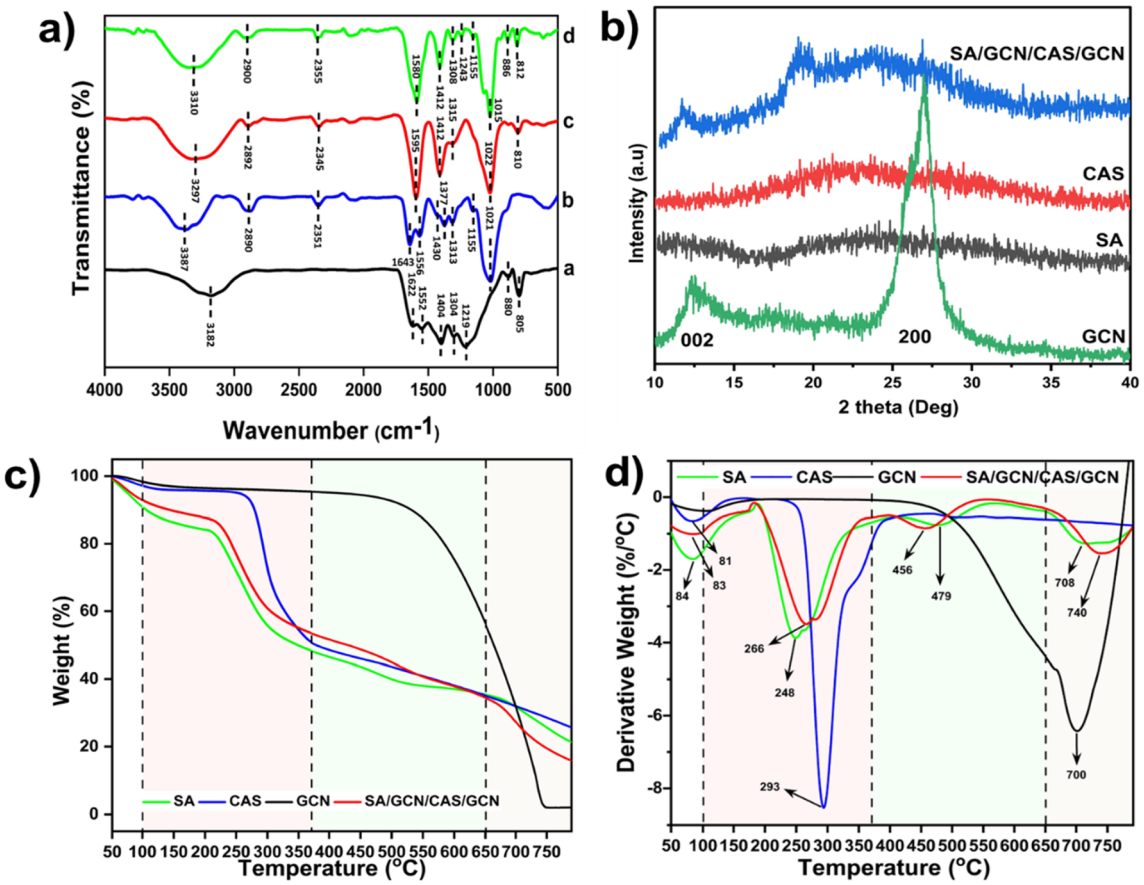

Fig. 5 (a) FTIR spectrum, (a) and (b) XRD graphs, (c) TGA and (d) DTG thermogram of GCN SA, CAS, and SA/GCN/CAS/GCN layer by layer coating.

from O–H stretching of hydroxyl groups involved in hydrogen bonding. Peaks at around 2890 cm^{-1} come from C–H stretching. The sharp peak at 1592 cm^{-1} is due to asymmetric stretching of carboxylate ($–COO^-$) groups, while the peak at 1412 cm^{-1} corresponds to their symmetric stretching.[15] The band at 1021 cm^{-1} comes from C–O–C stretching in the glycosidic bonds of the polymer.[46] The FTIR spectrum of chitosan (Fig. 5a–c) shows a broad peak at 3310 cm^{-1} from overlapping O–H and N–H stretching vibrations. Peaks at 2892 and 2345 cm^{-1} are due to C–H stretching and possible CO_2 impurities. The band near 1595 cm^{-1} indicates N–H bending of primary amines, while peaks at 1412 and 1315 cm^{-1} come from C–N stretching and CH_2 wagging. The peak at 1022 cm^{-1} is from C–O stretching in the glucosamine ring, and 810 cm^{-1} reflects vibrations of the sugar ring skeleton. A distinct N–H stretching peak is not clearly resolved due to strong hydrogen bonding and overlap with the broad O–H stretching region. The FTIR spectrum of the layer-by-layer coating (SA/GCN/CAS/GCN, Fig. 5a–c) shows features from all components and hints at interactions between them. The broad peak at 3310 cm^{-1} shows –OH and –NH groups from SA and CAS, with slight shifts and broadening indicating stronger hydrogen bonding. The carboxylate asymmetric stretch shifts from 1592 cm^{-1} in pure SA to 1580 cm^{-1}, suggesting ionic or coordination interactions between alginate carboxylates, CAS amines, or GCN nitrogen sites. The 1555–1308 cm^{-1} region shows overlapping C–N, C–O, and C=N vibrations, indicating hydrogen bonding and electrostatic interactions. The C–O–C peak at 1015 cm^{-1} is slightly shifted, supporting structural changes or bonding with GCN. Bands at 888 and 812 cm^{-1} confirm triazine and saccharide ring vibrations. Overall, combining GCN with SA and CAS induces structural changes through hydrogen bonding, electrostatic forces, and possibly coordination bonds among $–COO^-$, $–NH_2$, –OH, and C–N groups.[47,48]

4.3 X-ray diffraction (XRD) analysis

X-ray diffraction (XRD) was used to study the crystal structure and compatibility of GCN, SA, CAS, and the SA/GCN/CAS/GCN layer-by-layer coating, as shown in Fig. 5b. The XRD pattern of GCN shows a sharp peak at 27.4° (2θ), which comes from the stacked layers of its aromatic structure, and a smaller broad peak at about 13.1° from the in-plane tri-*s*-triazine units.[49] The strong 27.4° peak confirms that GCN has a well-ordered, layered graphitic structure. Sodium alginate (SA) shows a broad, low-intensity peak at around 21–22°, indicating it is mostly amorphous with flexible, disordered polysaccharide chains. Chitosan (CAS) shows a broad hump at around 20°, reflecting its semi-crystalline nature with partially ordered chains. The low intensity of this peak suggests that CAS has amorphous regions and hydrogen bonding between molecules.[50] The composite SA/GCN/CAS/GCN shows a broadened and less intense peak at 27°, corresponding to the GCN phase, while the typical sharp crystalline peak of GCN is significantly suppressed. Moreover, new broad features emerge between 13 and 25°, like at 27° due to interactions and partial phase blending between GCN and the biopolymer matrix. The lack of distinct crystalline peaks from chitosan or alginate suggests a high degree of structural integration, where hydrogen bonding and electrostatic interactions disrupt regular packing and reduce long-range order, confirming that GCN was successfully embedded and dispersed in the SA/CAS matrix, leading to amorphization and structural distortion of the crystalline GCN. This dispersion is helped by the positive amino groups of chitosan, the negative carboxyl groups of alginate, and the nitrogen groups of GCN, which attract each other through electrostatic interactions. Similar interfacial compatibilisation effects have been reported in other hybrid nanocomposite coatings.[51] GCN maintains high crystallinity in its pure form and its incorporation into the SA/GCN/CAS/GCN multilayer coating results in peak broadening and intensity reduction, indicating strong interfacial interactions and good dispersion. The amorphous behaviour of SA and CAS supports a flexible matrix capable of encapsulating and stabilizing GCN within a non-crystalline structure.

4.4 Thermogravimetric analysis (TGA) and DTG

The thermal stability of pure GCN and the composite-coated films was tested using thermogravimetric analysis (TGA) and DTG, as shown in Fig. 5c. The weight loss of the films occurs in four stages: room temperature to 200 °C, 200–370 °C, 370–650 °C, and above 650 °C. Below 200 °C, a small weight loss occurs due to evaporation of surface water, impurities, and crystal water, starting mainly at around 80–85 °C, as reported in previous studies.[52,53] Between 200 °C and 370 °C, the films lose about 35% of their weight because the polymer chains break, removing side –OH groups and undergoing other chemical changes like denaturation, decarboxylation, and decarbonylation.[54] Adding CAS and GCN increases the decomposition temperature from 247 °C (pure SA) to 266 °C, showing stronger chemical interactions, especially hydrogen bonds, that improve thermal stability. Between 370 °C and 650 °C, the remaining carbon-based materials degrade, and the maximum weight loss temperature shifts higher due to the fillers.[53,55] The LbL-coated film shows a slightly lower maximum weight loss temperature (456 °C) compared to pure SA (479 °C), with carbonisation forming char. After full degradation, the ash content is 21.3% for SA, 25.5% for CAS, 2% for GCN, and 15.7% for the composite films. Overall, adding CAS and GCN significantly improves thermal stability, which is important for protecting packaged foods during heat exposure in storage, transport, and handling.

4.5 Scanning electron microscopy (SEM)

The surface and cross-section of the layer-by-layer coating were examined using Scanning Electron Microscopy (SEM), as shown in Fig. 6. The SEM images reveal significant morphological distinctions among pristine sodium alginate (SA), pristine chitosan (CAS), and the LbL coating comprising (SA/GCN/CS/GCN). Fig. 6a illustrates the surface morphology of the pristine SA film. The surface appears relatively smooth and homogeneous, with no visible pores or phase separation, which is characteristic of ionotropically gelled sodium alginate networks.[56] Fig. 6b shows the SEM micrograph of CAS. Similar to SA, the CS film also exhibits a smooth and dense surface, lacking significant

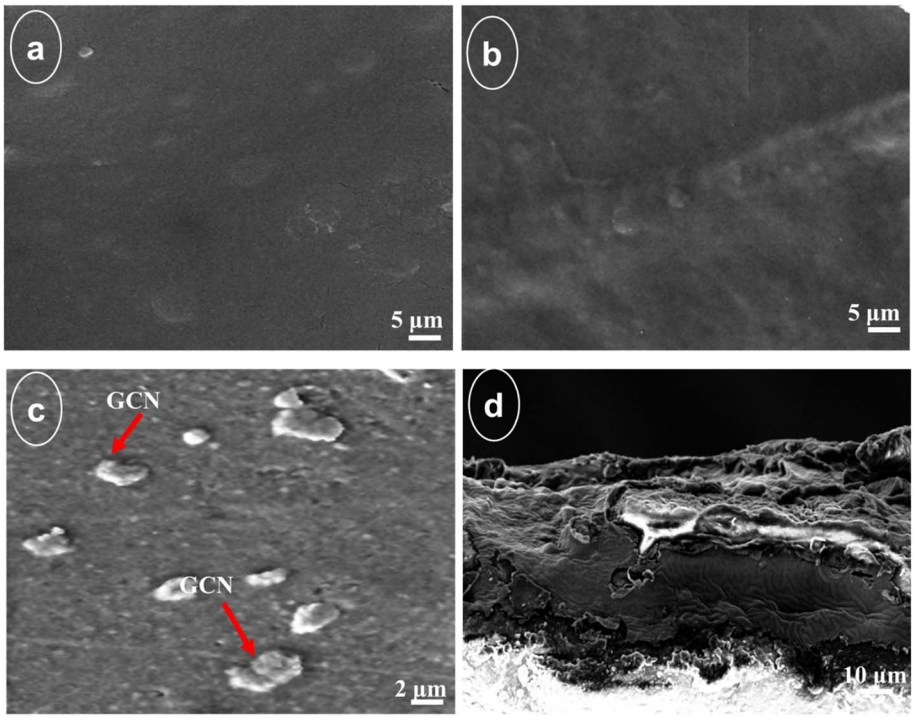

Fig. 6 SEM image of (a) SA, (b)CAS, (c)SA/GCN/CAS/GCN, and (d) the SA/GCN/CAS/GCN layer by layer coating cross-section view.

porosity. This structure shows that chitosan can form smooth films well, thanks to electrostatic forces and hydrogen bonds between its polymer chains.[56] The absence of observable defects suggests a uniform polymeric network, with a slightly rougher surface than alginate, possibly due to a lower degree of chain entanglement. In contrast, the surface morphology of the SA/GCN/CS/GCN LbL coating, shown in Fig. 6c, reveals distinct microstructural features. At a higher magnification, the image clearly shows multiple spots labelled as GCN, which correspond to GCN sheets embedded on the surface. The small clusters of GCN show that some GCN stays on the surface while some interacts with the polymer underneath. Adding GCN makes the material slightly uneven, but this can improve its properties, such as water interaction, light-based activity, and strength.[57,58] The even spread of GCN on the surface shows that it interacts well with both SA and CAS. These interactions likely occur through hydrogen bonds or electrostatic forces, as noted in earlier studies.[51] Fig. 6d shows the cross-section of the

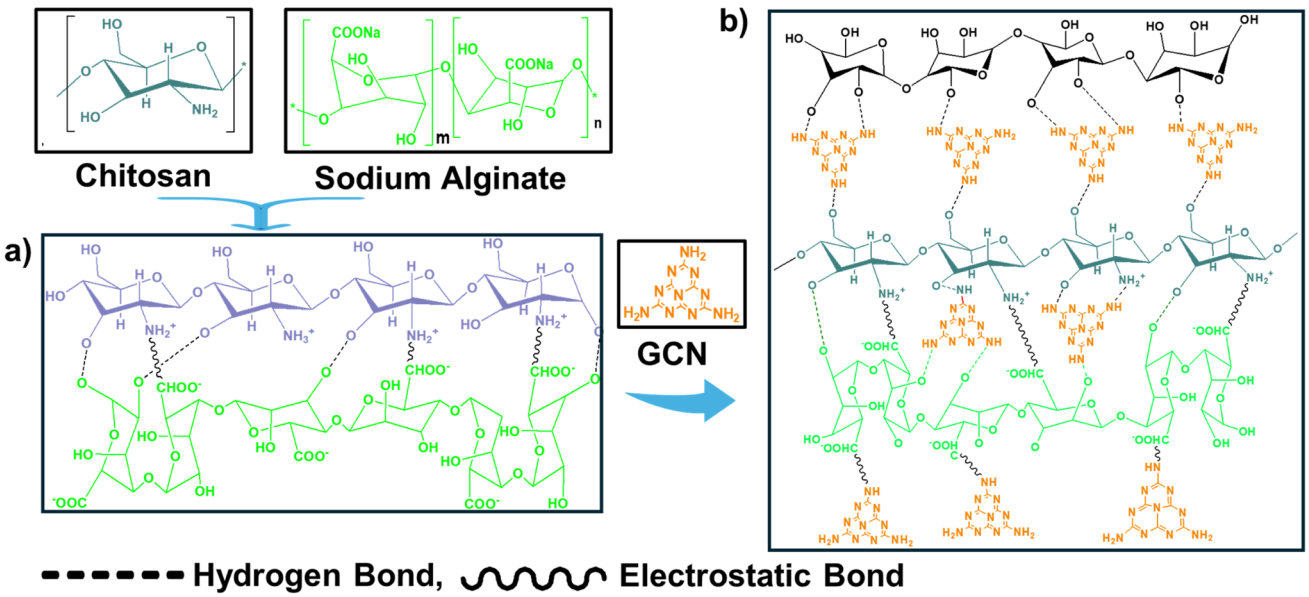

Fig. 7 Mechanism of interaction; (a) interaction between chitosan (CAS) and sodium alginate (SA), and (b) interaction among the chitosan (CAS), sodium alginate (SA), and graphitic carbon nitride (GCN).

composite membrane. The image displays a layered structure, proving that all the components are well combined. The GCN-containing layers look brighter, showing strong bonding between GCN and the polymer. The tightly packed structure means the layers are well mixed with little separation, which is important for the coating's stability. Fig. 7 illustrates how sodium alginate, chitosan, and graphitic carbon nitride interact with each other.

As shown in Fig. 8, the stability of GCN dispersions mainly depends on the type of liquid used to disperse them. In aqueous media, GCN nanosheets tend to agglomerate and eventually precipitate due to their intrinsic hydrophobicity and strong van der Waals interactions, which promote restacking and sedimentation over time. As previously reported, GCN exhibits limited colloidal stability in pure water, often resulting in significant sedimentation within 12 hours, particularly in the absence of stabilising agents or surface modifications.[59] However, when GCN is dispersed in polymeric matrices such as CAS and SA, its stability is markedly enhanced, with no visible precipitation observed for up to 72 hours. This improvement occurs because GCN interacts in many ways with the functional groups of the biopolymers. Chitosan, which has many amino groups, can attach to the negatively charged areas on the GCN surface through electrostatic forces and hydrogen bonds. Likewise, sodium alginate has carboxylate groups that can form hydrogen bonds or coordinate with the nitrogen-rich parts of GCN, as shown in Fig. 7. These interactions inhibit GCN restacking by steric and electrostatic stabilisation, forming a stable hybrid colloidal system.

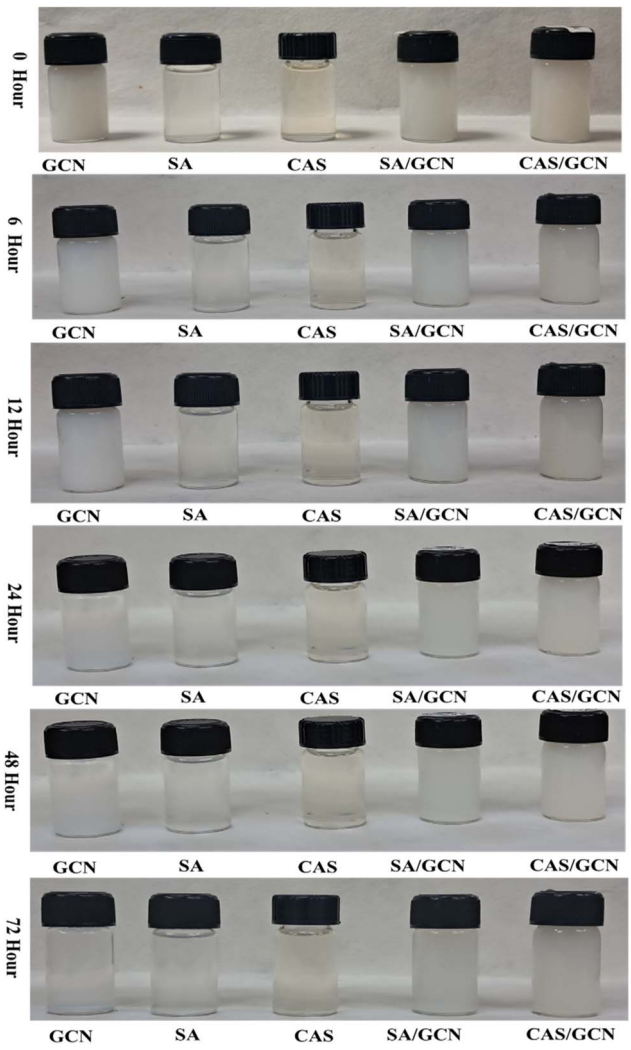

Fig. 8 Stability of GCN, SA, CAS, SA/GCN, and CAS/GCN coating solution.

4.6 Moisture content (MC), water solubility (WS) and swelling index (SI)

Moisture content (MC) was measured to understand how easily SA, CAS, and the SA/GCN/CAS/GCN coating absorb moisture from the environment. Both SA and CAS have water-attracting groups; SA contains hydroxyl and carboxyl groups, while CAS has hydroxyl and amine groups, which naturally draw in and hold water. As shown in Fig. 9a, both neat films exhibited relatively high MC values, with CAS showing a higher moisture content of 17.9% compared to that of SA, 13.9%. The incorporation of GCN as a nanofiller further reduced the MC of both SA and CAS films. This reduction can be explained in two ways. First, GCN works like a barrier that slows down water movement by breaking the continuous water-loving network of the polymer. Second, the crystalline structure of GCN makes the film more tightly packed, leaving less space and making it harder for water molecules to reach the hydrophilic groups.[60] Water solubility (WS) is another critical parameter for biodegradable films, especially in food and biomedical applications where water resistance is essential. As illustrated in Fig. 9a, the WS values for the films ranged between 2.5% and 10.6%, indicating that all formulations remained nearly insoluble even after 24 hours of water immersion. The addition of GCN significantly reduced WS across all films, suggesting enhanced water resistance. This can be linked to the denser and more compact polymer network formed due to GCN filler and crosslinking effects. The swelling index (SI) is shown in Fig. (9b), as it reflects the coating water uptake capacity and dimensional stability upon hydration, both of which are significant factors in food packaging. Swelling tests conducted over 2 hours revealed that neat CAS and SA coatings exhibited maximum swelling values of approximately 360% and 125%, respectively, after 120 minutes before reaching equilibrium. Swelling occurs when water enters the water-loving polymer structure. The water molecules form hydrogen bonds with groups like –OH, $–NH_2$, and –COOH, which causes the polymer chains to relax and expand.[61] On incorporation of GCN, a marked reduction in swelling was observed. This behaviour can be attributed to the dual role of GCN which serves as a hydrogen bonding partner and a physical crosslinking agent. g-C_3N_4 interacts with the polymer chains and limits their movement. This reduces the number of sites that can attract water, helping the material form a tighter structure that swells less. Similar results have been seen in other studies using nanofillers like ZnO, Ag, and TiO_2, which also make materials more stable by reducing water absorption.[62] Adding GCN makes the SA and CAS films better at resisting moisture, less likely to dissolve in water, and more stable in shape. These

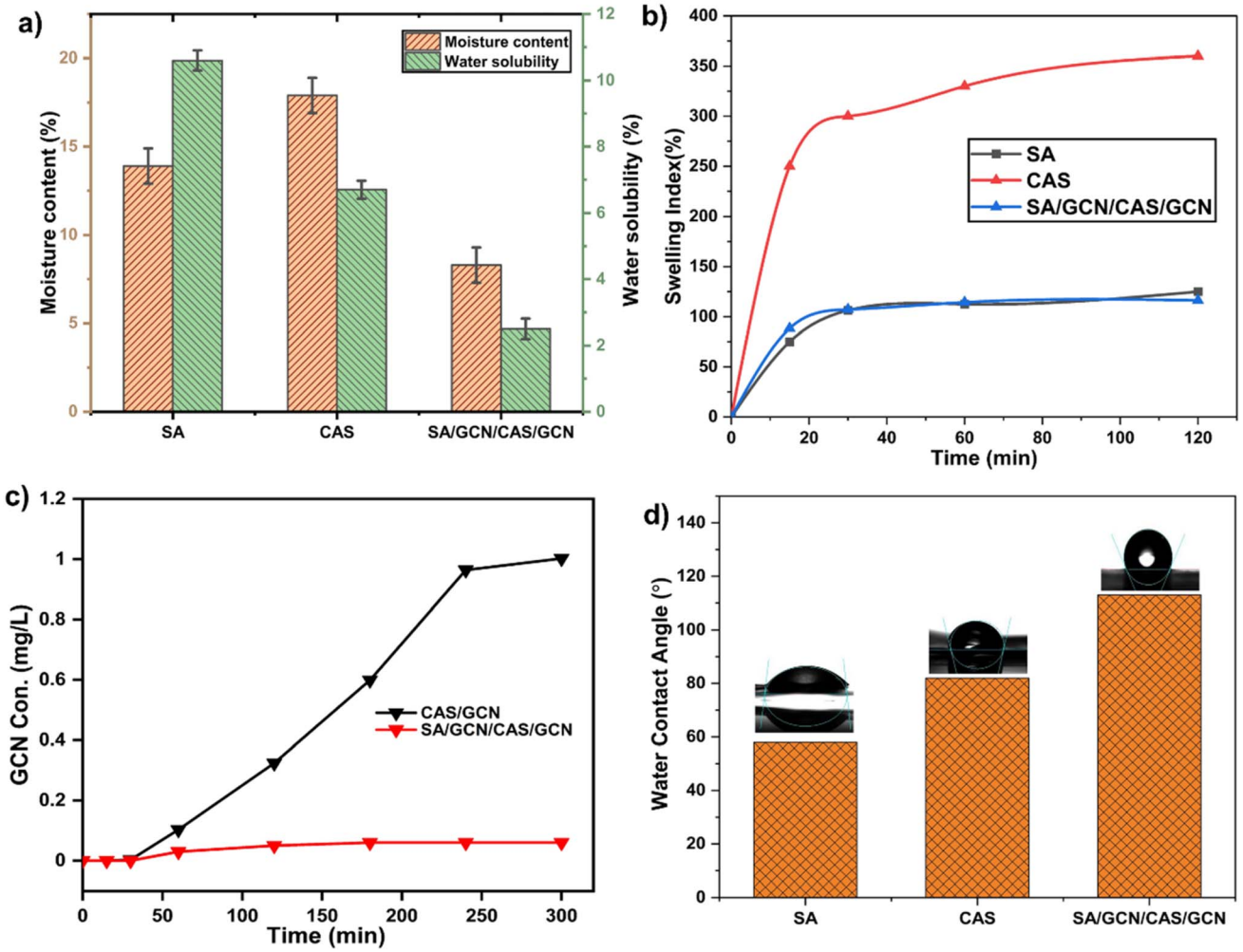

Fig. 9 (a)Moisture content (MC), water solubility (WS), (b)swelling index (SI), and (c) leaching behaviour of LbL coating.

improvements make the films more useful for packaging foods or making biomedical products that need protection from moisture.

4.7 Leaching behaviour of the coating

To check if the food coatings are safe and stable, we tested whether GCN could leak out from CAS/GCN and SA/GCN/CAS/GCN coatings. This was done using the TCLP following EPA Method 1311. This method mimics mildly acidic environmental conditions that food packaging materials might encounter. It is a good way to determine if contaminants might enter food or the surrounding environment. Fig. 9c shows that the two coatings leached in very different ways over the 300 minutes. The concentration of GCN in the CAS/GCN film gradually increased from approximately 0 mg L^{-1} to nearly 1.0 mg L^{-1}, indicating that GCN slowly leached into the solution, likely due to the weak retention capacity of the chitosan matrix. The CAS hydrophilic structure may help the leaching medium spread, which could help release embedded nanomaterials, as Hou *et al.* reported before.[63] The SA/GCN/CAS/GCN LbL coating had a consistently low level of GCN leaching, staying below 0.05 mg L^{-1}. This result demonstrates that the addition of an SA interlayer significantly enhances the coating structural integrity and resistance to leaching. The negatively charged SA and positively charged CAS attract each other strongly. This helps the film stay tight and stable, keeping the GCN particles in place.[64] The LbL design may also provide extra physical confinement, which would slow down the movement of nanoparticles. From a safety perspective, the minimal GCN release noted in the SA/GCN/CAS/GCN system indicates that this coating is appropriate for direct food-contact applications, presenting no risk to human health and the environment.

4.8 Water contact angle (WCA)

Fig. 9d presents the water contact angle (WCA) measurements of the SA, CAS, and LbL coating of SA/GCN/CAS/GCN. The WCA is a critical criterion for assessing the surface wettability of a coating, where higher contact angles indicate greater hydrophobicity. This property is particularly important in food coating applications, as increased hydrophobicity can reduce moisture transfer, and deter microbe-growth, and shelf life of

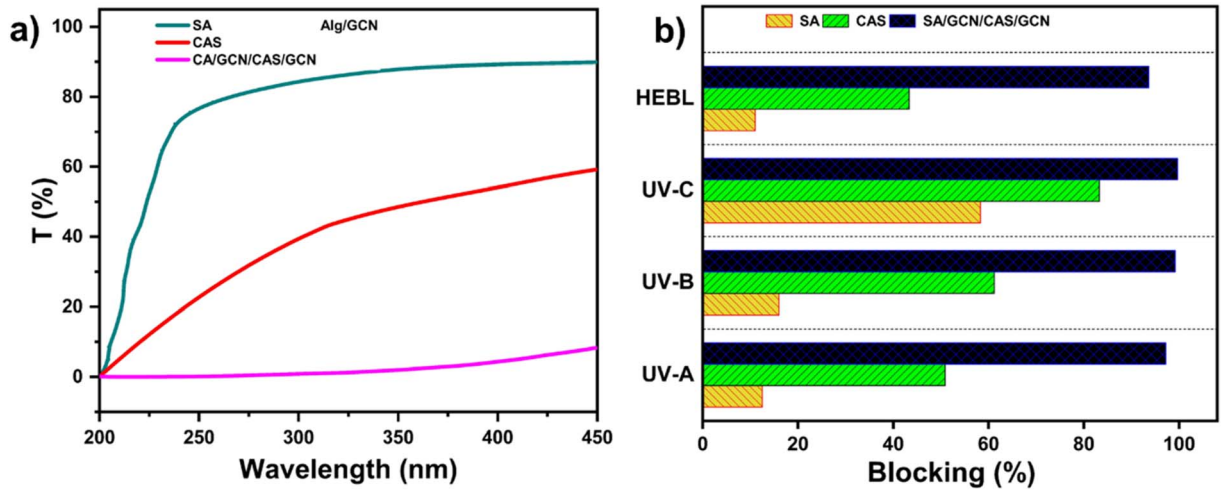

Fig. 10 UV and HEBL blocking characteristics of the SA, CAS, and SA/GCN/CAS/GCN LbL coating.

perishable foods. SA exhibits the lowest WCA (58°) among the samples, indicating its strong hydrophilic nature. This can be attributed to the abundant hydroxyl and carboxylate functional groups present in its structure, which readily interact with water molecules through hydrogen bonding. Although SA is commonly used in edible coatings because it is safe and can form films, it naturally attracts water. This makes it less effective for packaging foods that need protection from moisture.[65] On the other hand, CAS displays a moderately higher WCA (81°), reflecting reduced surface wettability. This improvement in hydrophobicity arises from the partial deacetylation of chitosan, which introduces amine groups that reduce the density of hydrophilic interactions. Chitosan films are also semi-crystalline in nature, which enhances their water resistance compared to purely amorphous SA films. Therefore, chitosan offers a superior moisture barrier performance and has been used extensively in antimicrobial food coating.[66] The layer-by-layer coating of the SA/GCN/CAS/GCN film demonstrates the highest WCA (113°), indicating a significant enhancement in surface hydrophobicity. This effect is primarily due to the incorporation of GCN, a 2D nanomaterial known for its low surface energy and high chemical stability. GCN not only makes the surface water-repellent through its π-conjugated structures but also makes it rougher. This roughness traps tiny air pockets under water droplets, creating a Cassie–Baxter wetting effect.[67] This structural modification results in reduced wettability and improved water barrier properties. Moreover, the LbL coating configuration creates a tortuous path for moisture diffusion, further enhancing the coating protective performance.[65,68]

4.9 UV and HEBL blocking properties of the coating

UV-visible transmittance spectra of SA, CAS and SA/GCN/CAS/GCN LbL coating were scrutinized for the determination of UV-blocking properties of the corresponding films, as depicted in Fig. 10. The transmittance profile of neat polymer SA and CAS coating exhibited lower UV blocking ability (SA: 85% transmittance of UV-A and UV-B, and 42% of UV-C; CAS: 26, 19.3, and 8.5% transmittance of UV-A, UV-B and UV-C, respectively. SA/GCN/CAS/GCN layer-by-layer coating showed lower transmittance compared to other respective polymer films in the UV region. Among these films, the SA/GCN/CAS/GCN layer by layer coating was particularly effective, blocking 97.2% of UV-A (320–400 nm) 99.2% of UV-B (280–320 nm), and 97.2% of UV-A (320–400 nm) 99.7% of UV-C (200–280 nm) regions. In addition to that, SA/GCN/CAS/GCN layer-by-layer coating was able to block approximately 94% of HEBL from solar irradiation. This can be attributed to the UV absorbance phenomena of the synthesised GCN as mentioned in Fig. 4e. The film can absorb solar UV radiation by π–π and n–π alteration within GCN.[39,40] In addition, the material has a flat, sheet-like structure made of connected hetero-aromatic rings. This structure helps protect against harmful UV rays by reflecting them away, preventing damage.[69] The addition of GCN to polymeric films, including polypropylene,[70] and polyvinyl alcohol (PVA),[71] has been reported in the literature as being effective for UV-blocking properties. These findings confirm that the GCN incorporating films exhibit excellent UV-blocking capabilities, making them highly beneficial for food packaging applications by preventing oxidation, discoloration, and other photolytic reactions.

4.10 Antimicrobial activity of the coating

Fig. 11 presents the zones of inhibition, with measurements carefully conducted using Image J software, showing a progressive enhancement in the antibacterial performance of the coating. The control-coated SA served as the baseline, exhibiting complete bacterial coverage with no visible zone of inhibition, consistent with the absence of antimicrobial functionality. This observation was corroborated by the colony-forming assay, in which both *E. coli* and *S. aureus* exhibited extensive growth, with counts exceeding 1000 colonies for each strain, confirming the lack of antibacterial activity in the SA film. However, SA/GCN exhibits a noticeable shift. The zone of inhibition expanded, reaching a zone area of 137 mm^2 for *E. coli* and 135 mm^2 for *S. aureus*, with the increased areas measuring 59 mm^2 and 57

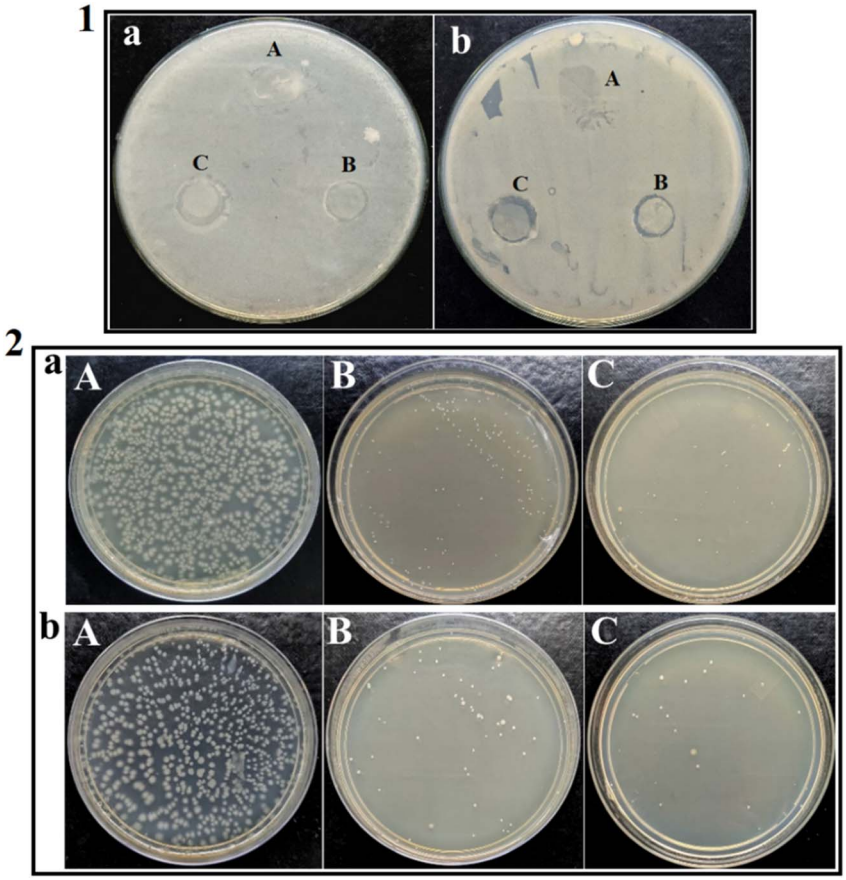

Fig. 11 Antimicrobial images (1 is disk diffusion assay and 2 is colony counting assay) of composite films where a is *E. coli*, and b is *S. aureus*, and A, B, and C indicate SA, SA/GCN, and SA/GCN/CAS/GCN LbL coating, respectively.

mm^2, respectively. This was a clear indication that GCN had imparted antibacterial activity, showing not just a visible improvement in the zone of inhibition but also a significant reduction in colony numbers. For instance, only 157 colonies of *E. coli* and 57 colonies of *S. aureus* were observed, translating into an impressive kill percentage of 88.04% for *E. coli* and 94.73% for *S. aureus*. The SA/GCN/CAS/GCN layer-by-layer coating exhibited a remarkable synergistic effect, resulting in a significant increase in both the zone area and antibacterial activity. The zone areas surged to 167 mm^2 for *E. coli* and 175 mm^2 for *S. aureus*, with increased areas of 89 mm^2 and 97 mm^2, respectively. The results from the colony counting assay were equally astonishing; only 35 colonies of *E. coli* and 30 colonies of *S. aureus* remained, corresponding to a staggering kill percentage of 97.33% and 97.22%, respectively. To obstruct bacterial growth, SA/GCN/CAS/GCN layer-by-layer is considered most efficient as the combination of GCN and CAS created antimicrobial properties. CAS plays a pivotal role in this enhancement. Chitosan (CAS), composed of repeating *N*-acetylglucosamine and glucosamine units, and the bacterial surface possess negative charge; this negative charge and amino acids from chitosan create an electrostatic bond that compromises membrane stability. This interaction, coupled with interference in DNA replication, increases membrane permeability and promotes leakage of intracellular constituents. This hampers the ability of bacteria to synthesize RNA and proteins, effectively shutting down their cellular machinery. On the other hand, the GCN-based substances in the coating also enhance photocatalytic antibacterial activity. Under visible light, GCN generates reactive oxygen species (ROS) that disrupt bacterial cell walls, further accelerating the killing process.[70–74] The combination of GCN and CAS in the layer-by-layer coating delivers not only superior antibacterial performance but also highlights the strength of their synergistic effect.[75,76] SA/GCN/CAS/GCN LbL not only outperformed the GCN embedded but also provided an exceptional level of bacterial resistance.

4.11 "*In vitro*" cytotoxicity study of the coating

An MTT assay was performed to test the biocompatibility of SA/GCN/CAS/GCN LbL coating as demonstrated in Fig. 12a on a HeLa mouse fibroblast cell line in an "*in vitro*" cytotoxicity test. The results showed that SA/GCN/CAS/GCN layer-by-layer coating had no adverse effect on fibroblast growth after being exposed for 24 hours. Dong *et al.*[77] showed that the cell viability was greater than 90% at all SA, CAS, and GCN concentrations, with no significant changes from the control. These findings are more encouraging; different coating types exhibit uneven results upon the same nanoparticle and bio-surface interaction. In this investigation, SA and CAS were employed as surface resilience and coating agents for the SA/GCN/CAS/GCN LbL coating. This

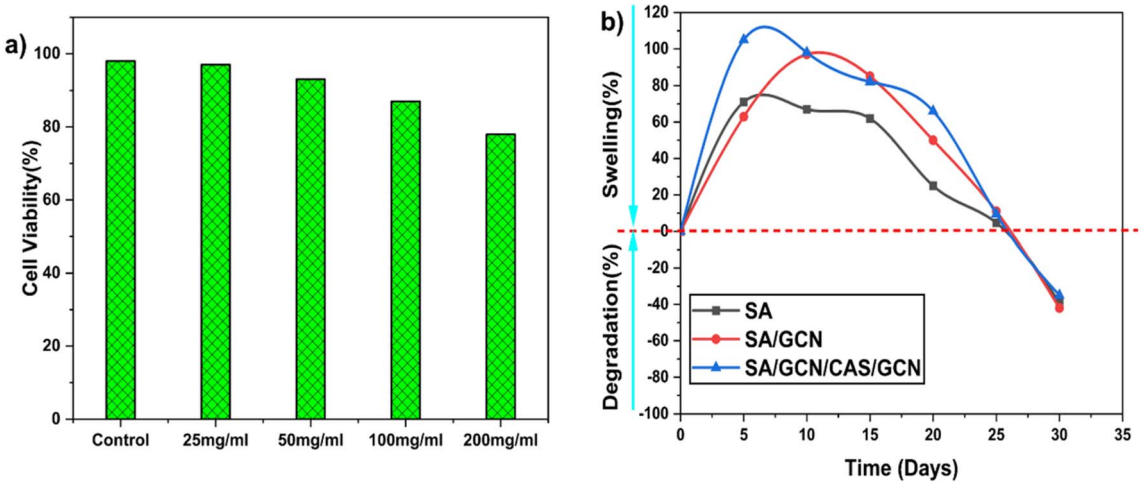

Fig. 12 (a) *In vitro* cytotoxicity of layer-by-layer coating of SA/GCN/CAS/GCN and (b) degradation of SA, SA/GCN, and SA/GCN/CAS/GCN layer-by-layer coating.

application effectively mitigated the leaching of GCN, thereby showcasing commendable biocompatibility. To keep the bio-surfaces out of electrostatic contact, surface coatings are necessary, and thereby surface charges of nanoparticles remain untouched. Additionally, they prevent extrinsic and intracellular components from damaging the GCN nanoparticles, thereby helping to maintain their biocompatibility. The high biocompatibility of the SA/GCN/CAS/GCN LbL coating shows that it is safe for food packaging.

4.12 Degradation behaviour of the coating

Swelling capacity of a material can be observed by using gravimetric weight gain/loss. The test was performed under wet conditions for 9 days and a gradual increase in swelling of the coated samples can be observed in Fig. 12b. Usually, polar groups like hydroxyl and carboxyl have strong water affinity, leading to swelling upon contact with moisture in the soil. The two polar groups are abundant in non-crosslinked SA and CAS; the swelling of the coated films might have occurred due to the crosslinking of SA polymer chains. Degradation of the multilayer edible-coated films became apparent after 9 days and continued progressively over a 30-day period. SA coating could break down initially due its weak crosslinking and stability of glycosidic bonds under hydrolytic conditions.[78] As a result, after 30 days, the SA coating degraded and the breakdown of the glycosidic link caused the primary polymer chain to break, which made the films less flexible and more brittle. The film exhibited several void spaces;

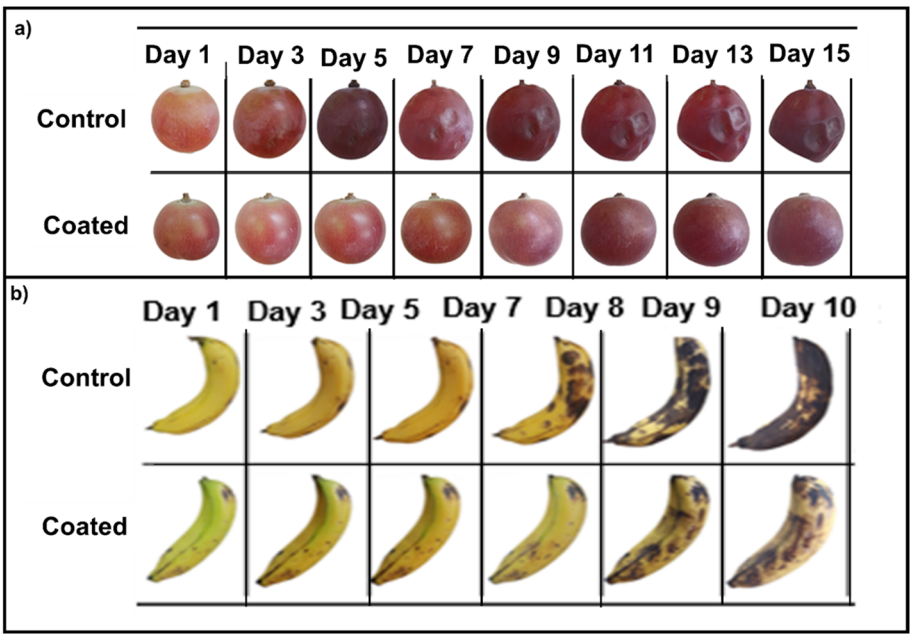

Fig. 13 Preservation of (a) red grape and (b) banana coated with SA/GCN/CAS/GCN layer-by-layer coating and compared with controlled uncoated samples. Shelf-life has been extended from 7 to 10 and 9 to 15 days for bananas and grapes, respectively.

blocks of monomeric acids were dominant in SA and it caused less crosslinking, as we know that blocks of gluconic acids result in better crosslinking. In addition, this low crosslinking of SA made it vulnerable to pH, water, bacteria, and microorganisms and other environmental factors.[79] Moreover, the incorporation of GCN in SA coating enhanced its degradation from 30% to 46%. The presence of GCN may have weakened the crosslinking process by disrupting the bonds between polymer chains and Ca^{2+}; thereby accelerating the film-breakdown. GCN may also have influenced the crystallinity and morphology of the polymer matrix, making it more amorphous. Amorphous regions tend to degrade more quickly than crystalline areas, contributing to an overall increase in degradation. Furthermore, the presence of CAS further intensified the degradation process. CAS, as shown in Fig. 2a, increases the swelling of the coated films, making them more vulnerable to moisture in the soil. This improved SA/GCN/CAS/GCN LbL coating makes it easier for water from the soil to get into the porous material through the network, which weakens the polymer chains.[80] Therefore, because there are more hydrolysis reactions in SA/GCN/CAS/GCN layer-by-layer coating, SA/GCN and SA-coated break down 25% faster than the SA coating.

4.13 Food preservation application

In order to evaluate shelf life/food preservation capability of the composite-SA/GCN/CAS/GCN LbL, grapes-red and bananas were chosen as samples, subsequently, and Fig. 13 depicts the difference in results while comparing the composite with the control. The standard prerequisites of storing the samples were temperature – 37 °C and relative humidity – 60%. Over time, both control samples exhibited increased wilting and shrinkage, which can be attributed to water loss through water vapour permeation from the surrounding environment. The durability of the SA/GCN/CAS/GCN LbL coating was demonstrated in experiments and is displayed in Fig. 13a and b, as the fruits covered with this SA/GCN/CAS/GCN LbL coating remained intact and exhibited a smooth surface even after 15 days for the grape sample and 10 days for the banana sample. This impressive performance is due to the SA/GCN/CAS/GCN LbL coating's ability to restrict the passage of water vapour, as previously noted. Based on the above discussion, a probable mechanism of food protection from UV radiation and microorganisms is illustrated in Fig. 13. In addition to the fruits and vegetables listed above, biopolymer composite films have also been shown to be effective in preserving other foods, such as

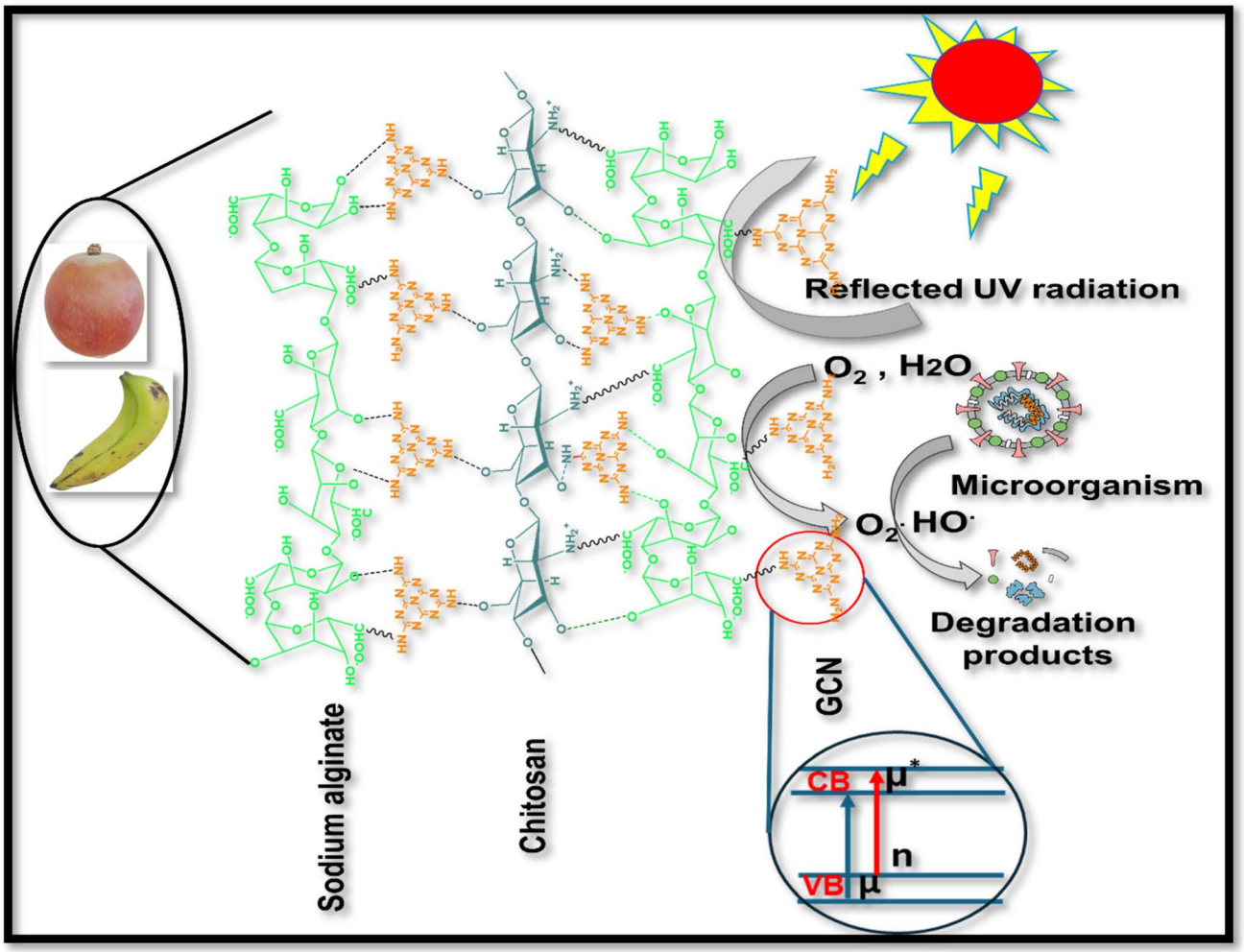

Fig. 14 Mechanism of food protection against microorganisms through radical scavenging and UV reflection.

Table 1 Comparative shelf-life performance of the SA/GCN/CAS/GCN LbL coating relative to recently reported coatings

Coating (biopolymer/Additives)	Fruits	Shelf life	References
Banana-starch/Chitosan/Aloe vera gel	Strawberries	Delayed decay; shelf-life extended by 6 days	81
Zein/PEO/Hexanal	Peach	Shelf-life extended 4 days (at ambient temperature, 0% RH)	82
Chitosan nanoparticle/TiO_2	Blueberries	Quality is maintained up to 8 days	83
Carrageenan/CMC blend	Banana	Extended shelf life 6–7 days	84
SA/GCN/CAS/GCN LbL coating	Banana/Red grape	Shelf-life has been extended from 7 to 10 and 9 to 15 days for bananas and grapes	This work***

meat, fish, and dairy products. Furthermore, the mechanism of food protection against microorganisms through radical scavenging and UV reflection is illustrated in Fig. 14. In conclusion, this study demonstrates that the SA/GCN/CAS/GCN LbL biopolymer coating offers a promising strategy for extending the shelf life of fruits and vegetables. Owing to its biodegradability, biocompatibility, and non-toxicity, this coating provides a sustainable alternative to conventional plastic films. The findings suggest that such biopolymer-based multilayer systems could play a significant role in advancing environmentally friendly food packaging solutions and reducing reliance on synthetic plastics (Table 1).

5. Conclusion

In this study, a novel, eco-friendly, and multifunctional LbL coating composed of sodium SA, CAS, and graphitic carbon nitride (GCN) was successfully developed for increasing the shelf life of perishable fruits. The inclusion of GCN into the SA/CAS matrix imparted significant enhancements in UV shielding, antimicrobial efficacy, water barrier properties, and ethylene scavenging, critical parameters for post-harvest fruit preservation. Structural analyses confirmed strong intermolecular interactions and homogeneous dispersion of GCN within the biopolymer network, leading to improved thermal stability, reduced moisture permeability, and minimal nanofiller leaching. The functional performance of the coating was further evidenced by its better UV and HEBL blocking capacity, with over UV-C 99.7% UV-B 99%, and 97% UV-A attenuation. This shielding protects fresh produce from photooxidation and microbial growth induced by solar radiation. Water solubility, swelling index, and moisture content assessments highlighted the coating's ability to act as an effective water barrier, while water contact angle (WCA) measurements (up to 113°) confirmed improved surface hydrophobicity, which is essential for reducing moisture-induced spoilage. The LbL coating demonstrated outstanding antibacterial activity, achieving over 97% inhibition against both Gram-negative and Gram-positive bacteria, while maintaining cell viability above 95%, affirming its biocompatibility and safety for direct food contact. Importantly, coated fruits showed a remarkable shelf-life extension of up to 15 days for grapes and 10 days for bananas without compromising quality. Extensive migration studies are required to ensure that GCN nanoparticles do not leach into the fruit pulp. The coating showed excellent biodegradability under soil burial conditions, emphasizing its potential as a sustainable alternative to conventional plastic-based packaging. To the best of our knowledge, this is the first report demonstrating the use of GCN as a functional nanofiller in biodegradable edible coatings, offering a scalable, safe, and environmentally sustainable strategy to address the global challenges of food spoilage and plastic waste. Although the GCN incorporating biopolymer composite LbL assembled coating exhibits a range of attractive and versatile properties and is often cited as non-toxic, it lacks widespread GRAS (Generally Recognized as Safe) certification for direct food contact in many jurisdictions.

Conflicts of interest

The authors declare that they have no known competing financial or personal interests that could have influenced the work reported in this paper.

Data availability

All data generated or analysed during this study are included in this published article. Additionally, datasets supporting the findings, such as raw characterization files (FTIR, XRD, SEM, TGA, and UV-vis spectra) and experimental measurements of antimicrobial and biodegradation tests, are available from the corresponding author upon reasonable request. No proprietary or restricted data were used in this study.

References

1 Q. Wang, W. Chen, W. Zhu, D. J. McClements, X. Liu and F. Liu, A Review of Multilayer and Composite Films and Coatings for Active Biodegradable Packaging, *npj Sci. Food*, 2022, **6**(1), 18, DOI: 10.1038/s41538-022-00132-8.
2 M. Qiao, Q. Liu, Y. Yong, Y. Pardo, R. Worobo, Z. Liu, S. Jiang and M. Ma, Scalable and Rechargeable Antimicrobial Coating for Food Safety Applications, *J. Agric. Food Chem.*, 2018, **66**(43), 11441–11450, DOI: 10.1021/acs.jafc.8b03864.
3 L. Al-Naamani, S. Dobretsov and J. Dutta, Chitosan-Zinc Oxide Nanoparticle Composite Coating for Active Food Packaging Applications, *Innov. Food Sci. Emerg. Technol.*, 2016, **38**, 231–237, DOI: 10.1016/j.ifset.2016.10.010.

4 A. Sirelkhatim, S. Mahmud, A. Seeni, N. H. M. Kaus, L. C. Ann, S. K. M. Bakhori, H. Hasan and D. Mohamad, Review on Zinc Oxide Nanoparticles: Antibacterial Activity and Toxicity Mechanism, *Nano-Micro Lett.*, 2015, **7**(3), 219–242, DOI: 10.1007/s40820-015-0040-x.

5 H. E. Salama and M. S. Abdel Aziz, Novel Biocompatible and Antimicrobial Supramolecular O-Carboxymethyl Chitosan Biguanidine/Zinc Physical Hydrogels, *Int. J. Biol. Macromol.*, 2020, **163**, 649–656, DOI: 10.1016/j.ijbiomac.2020.07.029.

6 M. S. Abdel Aziz, H. E. Salama and G. R. Saad, Diglycidyl Ether of Bisphenol A/Chitosan-Graft-Polyaniline Composites with Electromagnetic Interference Shielding Properties: Synthesis, Characterization, and Curing Kinetics, *Polym. Eng. Sci.*, 2019, **59**(2), 372–381, DOI: 10.1002/pen.24933.

7 M. S. A. Aziz and H. E. Salama, Developing Multifunctional Edible Coatings Based on Alginate for Active Food Packaging, *Int. J. Biol. Macromol.*, 2021, **190**, 837–844, DOI: 10.1016/j.ijbiomac.2021.09.031.

8 M. Mehedi Hasan, M. Nuruzzaman Khan, P. Haque and M. M. Rahman, Novel Alginate-Di-Aldehyde Cross-Linked Gelatin/Nano-Hydroxyapatite Bioscaffolds for Soft Tissue Regeneration, *Int. J. Biol. Macromol.*, 2018, **117**, 1110–1117, DOI: 10.1016/j.ijbiomac.2018.06.020.

9 M. M. Hasan, D. Islam and T. U. Rashid, Biopolymer-Based Electrolytes for Dye-Sensitized Solar Cells: A Critical Review, *Energy Fuel.*, 2020, **34**(12), 15634–15671, DOI: 10.1021/acs.energyfuels.0c03396.

10 N. A. Mukta, M. D. Islam, R. B. Dina, W. Haque and P. Haque, Radiation Processed Polysaccharides in Food Production, Preservation and Packaging Applications, *Radiation-Processed Polysaccharides*, 2022, pp. 107–154, DOI: 10.1016/B978-0-323-85672-0.00002-7.

11 M. N. Khan, M. M. Hasan, M. S. Islam, S. Biswas, T. U. Rashid, A. K. Mallik, A. Zaman, S. Sharmeen, P. Haque and M. M. Rahman, Biomimetic Gelatin Nanocomposite as a Scaffold for Bone Tissue Repair. in *Handbook of Composites from Renewable Materials*, 2017, pp 487–525, DOI: 10.1002/9781119441632.ch166.

12 M. M. Hasan, A. H. Chisty, M. M. Rahman and M. N. Khan, Bioprotein Based IPN Nanoparticles as Potential Vehicles for Anticancer Drug Delivery: Fabrication Technology, in *Interpenetrating Polymer Network: Biomedical Applications*, 2020, pp 183–203, DOI: 10.1007/978-981-15-0283-5_7.

13 M. C. Reyes-Avalos, R. Minjares-Fuentes, A. Femenia, J. C. Contreras-Esquivel, A. Quintero-Ramos, J. R. Esparza-Rivera and J. A. Meza-Velázquez, Application of an Alginate–Chitosan Edible Film on Figs (Ficus Carica): Effect on Bioactive Compounds and Antioxidant Capacity, *Food Bioprocess Technol.*, 2019, **12**(3), 499–511, DOI: 10.1007/s11947-018-2226-y.

14 M. C. Reyes-Avalos, A. Femenia, R. Minjares-Fuentes, J. C. Contreras-Esquivel, C. N. Aguilar-González, J. R. Esparza-Rivera and J. A. Meza-Velázquez, Improvement of the Quality and the Shelf Life of Figs (Ficus Carica) Using an Alginate–Chitosan Edible Film, *Food Bioprocess Technol.*, 2016, **9**(12), 2114–2124, DOI: 10.1007/s11947-016-1796-9.

15 S. N. Mousavi, H. Daneshvar, M. S. Seyed Dorraji, Z. Ghasempour, V. Panahi-Azar and A. Ehsani, Starch/Alginate/Cu-g-C3N4 Nanocomposite Film for Food Packaging, *Mater. Chem. Phys.*, 2021, **267**, 124583, DOI: 10.1016/j.matchemphys.2021.124583.

16 A. Žiūkaitė, M. Strykaitė and J. Damašius, Screening of Cellulose/Alginate Biocomposites for Waterproof Food Packaging, *J. Nat. Fibers*, 2022, 1–12, DOI: 10.1080/15440478.2022.2030847.

17 C. Ruan, Y. Zhang, J. Wang, Y. Sun, X. Gao, G. Xiong and J. Liang, Preparation and Antioxidant Activity of Sodium Alginate and Carboxymethyl Cellulose Edible Films with Epigallocatechin Gallate, *Int. J. Biol. Macromol.*, 2019, **134**, 1038–1044, DOI: 10.1016/j.ijbiomac.2019.05.143.

18 P. Thivya, Y. K. Bhosale, S. Anandakumar, V. Hema and V. R. Sinija, Development of Active Packaging Film from Sodium Alginate/Carboxymethyl Cellulose Containing Shallot Waste Extracts for Anti-Browning of Fresh-Cut Produce, *Int. J. Biol. Macromol.*, 2021, **188**, 790–799, DOI: 10.1016/j.ijbiomac.2021.08.039.

19 A. Pavinatto, A. V. de Almeida Mattos, A. C. G. Malpass, M. H. Okura, D. T. Balogh and R. C. Sanfelice, Coating with Chitosan-Based Edible Films for Mechanical/Biological Protection of Strawberries, *Int. J. Biol. Macromol.*, 2020, **151**, 1004–1011, DOI: 10.1016/j.ijbiomac.2019.11.076.

20 M. D. Islam, S. Rahaman, J. H. Jiban and M. M. Mahdi, Removal of Chromium from Aqueous Solution Using Chitosan: An Experimental Study, *Bulg. Chem. Commun.*, 2019, **51**(4), 618–624, DOI: 10.34049/bcc.51.4.5141.

21 M. M. Islam, S. Biswas, M. S. Islam, M. Shahruzzaman, M. M. Hasan, M. D. Islam, P. Haque and M. M. Rahman, Chitosan-Based Gels for Ocular Drug Delivery, *Mar. Biomater.*, 2022, 281–315, DOI: 10.1007/978-981-16-4787-1_9.

22 M. D. Islam, S. Rahaman, J. H. Jiban and M. M. Mahdi, Removal of Chromium from Aqueous Solution Using Chitosan: An Experimental Study, *Bulg. Chem. Commun.*, 2019, **51**(4), 618–624, DOI: 10.1039/C2RA00006G.

23 S. Sharma, P. Sanpui and S. Sankar, Fabrication of Antibacterial Silver Nanoparticle—Sodium Alginate–Chitosan Composite Films, *RSC Adv.*, 2012, **2**(13), 5837–5843, DOI: 10.1039/C2RA00006G.

24 S. Lazar, O. Garcia-Valdez, E. Kennedy, P. Champagne, M. Cunningham and J. Grunlan, Crosslinkable-Chitosan-Enabled Moisture-Resistant Multilayer Gas Barrier Thin Film, *Macromol. Rapid Commun.*, 2019, **40**(6), 1–5, DOI: 10.1002/marc.201800853.

25 R. Sun, J. Zhu, H. Wu, S. Wang, W. Li and Q. Sun, Modulating Layer-by-Layer Assembled Sodium Alginate-Chitosan Film Properties through Incorporation of Cellulose Nanocrystals with Different Surface Charge Densities, *Int. J. Biol. Macromol.*, 2021, **180**, 510–522, DOI: 10.1016/j.ijbiomac.2021.03.092.

26 N. Nowak, W. Grzebieniarz, G. Khachatryan, K. Khachatryan, A. Konieczna-Molenda, M. Krzan and J. Grzyb, Synthesis of Silver and Gold Nanoparticles in Sodium Alginate Matrix

Enriched with Graphene Oxide and Investigation of Properties of the Obtained Thin Films, *Appl. Sci.*, 2021, **11**(9), 3857, DOI: 10.3390/app11093857.

27 H. E. Salama and M. S. A. Aziz, Optimized Carboxymethyl Cellulose and Guanidinylated Chitosan Enriched with Titanium Oxide Nanoparticles of Improved UV-Barrier Properties for the Active Packaging of Green Bell Pepper, *Int. J. Biol. Macromol.*, 2020, **165**, 1187–1197, DOI: 10.1016/j.ijbiomac.2020.09.254.

28 S. A. A. Mohamed, M. El-sakhawy and M. A. El-sakhawy, Polysaccharides, Protein and Lipid -Based Natural Edible Films in Food Packaging: A Review, *Carbohydr. Polym.*, 2020, **238**, 116178, DOI: 10.1016/j.carbpol.2020.116178.

29 S. Shankar and J. W. Rhim, Preparation of Sulfur Nanoparticle-Incorporated Antimicrobial Chitosan Films, *Food Hydrocoll.*, 2018, **82**, 116–123, DOI: 10.1016/j.foodhyd.2018.03.054.

30 R. Priyadarshi, H. J. Kim and J. W. Rhim, Effect of Sulfur Nanoparticles on Properties of Alginate-Based Films for Active Food Packaging Applications, *Food Hydrocoll.*, 2021, **110**, 106155, DOI: 10.1016/j.foodhyd.2020.106155.

31 L. Cui, T. Pu, X. Fang, J. Song, S. Li, J. Wang, C. Yin, H. Shi and S. Kang, Graphitic Carbon Nitride Sputtered with Silver Nanoparticles for Efficient Photocatalytic Degradation of Rhodamine B Dye, *Int. J. Electrochem. Sci.*, 2018, **13**(5), 4981–4990, DOI: 10.20964/2018.05.83.

32 T. U. Rashid, M. M. Rahman, S. Kabir, S. M. Shamsuddin and M. A. Khan, A New Approach for the Preparation of Chitosan from γ-Irradiation of Prawn Shell: Effects of Radiation on the Characteristics of Chitosan, *Polym. Int.*, 2012, **61**(8), 1302–1308, DOI: 10.1002/pi.4207.

33 X. Zhang, G. Xiao, Y. Wang, Y. Zhao, H. Su and T. Tan, Preparation of Chitosan-TiO2 Composite Film with Efficient Antimicrobial Activities under Visible Light for Food Packaging Applications, *Carbohydr. Polym.*, 2017, **169**, 101–107, DOI: 10.1016/j.carbpol.2017.03.073.

34 M. Yadav, P. Goswami, K. Paritosh, M. Kumar, N. Pareek and V. Vivekanand, Seafood Waste: A Source for Preparation of Commercially Employable Chitin/Chitosan Materials, *Bioresour. Bioprocess.*, 2019, **6**(1), 8, DOI: 10.1186/s40643-019-0243-y.

35 K. Divya and M. S. Jisha, Chitosan Nanoparticles Preparation and Applications, *Environ. Chem. Lett.*, 2018, **16**, 101–112, DOI: 10.1007/s10311-017-0670-y.

36 Q. Su, J. Sun, J. Wang, Z. Yang, W. Cheng and S. Zhang, Urea-Derived Graphitic Carbon Nitride as an Efficient Heterogeneous Catalyst for CO2 Conversion into Cyclic Carbonates, *Catal. Sci. Technol.*, 2014, **4**(6), 1556–1562, DOI: 10.1039/c3cy00921a.

37 M. I. Chebanenko, A. A. Lobinsky, V. N. Nevedomskiy and V. I. Popkov, NiO-Decorated Graphitic Carbon Nitride toward Electrocatalytic Hydrogen Production from Ethanol, *Dalton Trans.*, 2020, **49**(34), 12088–12097, DOI: 10.1039/d0dt01602k.

38 K. C. Christoforidis, T. Montini, E. Bontempi, S. Zafeiratos, J. J. D. Jaén and P. Fornasiero, Synthesis and Photocatalytic Application of Visible-Light Active β-Fe2O3/g-C3N4 Hybrid Nanocomposites, *Appl. Catal., B*, 2016, **187**, 171–180, DOI: 10.1016/j.apcatb.2016.01.013.

39 I. S. Pieta, A. Lewalska-Graczyk, P. Pieta, G. Garbarino, G. Busca, M. Holdynski, G. Kalisz, A. Sroka-Bartnicka, R. Nowakowski, M. Naushad, M. B. Gawande and R. Zbořil, Graphitic Carbon Nitride-Nickel Catalyst: From Material Characterization to Efficient Ethanol Electrooxidation, *ACS Sustain. Chem. Eng.*, 2020, **8**(18), 7244–7255, DOI: 10.1021/acssuschemeng.0c02267.

40 H. Dai, X. Gao, E. Liu, Y. Yang, W. Hou, L. Kang, J. Fan and X. Hu, Synthesis and Characterization of Graphitic Carbon Nitride Sub-Microspheres Using Microwave Method under Mild Condition, *Diamond Relat. Mater.*, 2013, **38**, 109–117, DOI: 10.1016/j.diamond.2013.06.012.

41 B. K. Barman, Ø. Sele Handegård, A. Hashimoto and T. Nagao, Carbon Dot/Cellulose-Based Transparent Films for Efficient UV and High-Energy Blue Light Screening, *ACS Sustain. Chem. Eng.*, 2021, **9**(29), 9879–9890, DOI: 10.1021/acssuschemeng.1c02791.

42 A. A. Dehkharghani, Exfoliated Graphitic Carbon Nitride for the Fast Adsorption of Metal Ions from Acid Mine Drainage : A Case Study from the Sungun Copper Mine, *Mine Water Environ.*, 2019, **38**(2), 335–341.

43 J. Wang, M. Li, M. Qian, S. Zhou, A. Xue, L. Zhang, Y. Zhao and W. Xing, Simple Synthesis of High Specific Surface Carbon Nitride for Adsorption-Enhanced Photocatalytic Performance, *Nanoscale Res. Lett.*, 2018, **13**(1), 248.

44 M. Xu, L. Han and S. Dong, Facile Fabrication of Highly Efficient G-C3N4/Ag2O Heterostructured Photocatalysts with Enhanced Visible-Light Photocatalytic Activity, *ACS Appl. Mater. Interfaces*, 2013, **5**, 12533–12540, DOI: 10.1021/am4038307.

45 D. Zhou and C. Qiu, Study on the Effect of Co Doping Concentration on Optical Properties of G-C3N4, *Chem. Phys. Lett.*, 2019, **728**, 70–73, DOI: 10.1016/j.cplett.2019.04.060.

46 H. Aloui, K. Khwaldia, L. Sánchez-González, L. Muneret, C. Jeandel, M. Hamdi and S. Desobry, Alginate Coatings Containing Grapefruit Essential Oil or Grapefruit Seed Extract for Grapes Preservation, *Int. J. Food Sci. Technol.*, 2014, **49**(4), 952–959, DOI: 10.1111/ijfs.12387.

47 X. Kong, X. Liu, Y. Zheng, P. K. Chu, Y. Zhang and S. Wu, Graphitic Carbon Nitride-Based Materials for Photocatalytic Antibacterial Application, *Mater. Sci. Eng., R*, 2021, **145**, 100610, DOI: 10.1016/j.mser.2021.100610.

48 M. Dash, F. Chiellini, R. M. Ottenbrite and E. Chiellini, Chitosan—A Versatile Semi-Synthetic Polymer in Biomedical Applications, *Prog. Polym. Sci.*, 2011, **36**(8), 981–1014, DOI: 10.1016/j.progpolymsci.2011.02.001.

49 X. Wang, K. Maeda, A. Thomas, K. Takanabe, G. Xin, J. M. Carlsson, K. Domen and M. Antonietti, A Metal-Free Polymeric Photocatalyst for Hydrogen Production from Water under Visible Light, *Nat. Mater.*, 2009, **8**(1), 76–80, DOI: 10.1038/nmat2317.

50 I. Younes and M. Rinaudo, Chitin and Chitosan Preparation from Marine Sources. Structure, Properties and

Applications, *Mar. Drugs*, 2015, 1133–1174, DOI: 10.3390/md13031133.

51 S. Ardebilchi Marand, H. Almasi and N. Ardebilchi Marand, Chitosan-Based Nanocomposite Films Incorporated with NiO Nanoparticles: Physicochemical, Photocatalytic and Antimicrobial Properties, *Int. J. Biol. Macromol.*, 2021, **190**, 667–678, DOI: 10.1016/j.ijbiomac.2021.09.024.

52 Z. Han, N. Wang, H. Fan and S. Ai, Ag Nanoparticles Loaded on Porous Graphitic Carbon Nitride with Enhanced Photocatalytic Activity for Degradation of Phenol, *Solid State Sci.*, 2017, **65**, 110–115, DOI: 10.1016/j.solidstatesciences.2017.01.010.

53 W. Zhao, Y. Qi, Y. Wang, Y. Xue, P. Xu, Z. Li and Q. Li, Morphology and Thermal Properties of Calcium Alginate/Reduced Graphene Oxide Composites, *Polymers*, 2018, **10**(9), 1–11, DOI: 10.3390/polym10090990.

54 C. J. Zhang, Y. Liu, L. Cui, C. Yan and P. Zhu, Bio-Based Calcium Alginate Nonwoven Fabrics: Flame Retardant and Thermal Degradation Properties, *J. Anal. Appl. Pyrolysis*, 2016, **122**, 13–23, DOI: 10.1016/j.jaap.2016.10.030.

55 Y. Shi, S. Jiang, K. Zhou, C. Bao, B. Yu, X. Qian, B. Wang, N. Hong, P. Wen, Z. Gui, Y. Hu and R. K. K. Yuen, Influence of G-C3N4 Nanosheets on Thermal Stability and Mechanical Properties of Biopolymer Electrolyte Nanocomposite Films: A Novel Investigation, *ACS Appl. Mater. Interfaces*, 2014, **6**(1), 429–437, DOI: 10.1021/am4044932.

56 J.-W. Rhim, H.-M. Park and C.-S. Ha, Bio-Nanocomposites for Food Packaging Applications, *Prog. Polym. Sci.*, 2013, **38**(10), 1629–1652, DOI: 10.1016/j.progpolymsci.2013.05.008.

57 M. Zheng, M. Guo, F. Ma, W. Li and Y. Shao, Recent Advances in Graphitic Carbon Nitride-Based Composites for Enhanced Photocatalytic Degradation of Rhodamine B: Mechanism, Properties and Environmental Applications, *Nanoscale Adv.*, 2025, **7**(16), 4780–4802, DOI: 10.1039/D5NA00439J.

58 C. Wu, Q. Han and L. Qu, Functional Group Defect Design in Polymeric Carbon Nitride for Photocatalytic Application, *APL Mater.*, 2020, **8**(12), 120703, DOI: 10.1063/5.0029374.

59 X. Song, D. Tang, Y. Chen, M. Yin, Q. Yang, Z. Chen and L. Zhou, A Facile and Green Combined Strategy for Improving Photocatalytic Activity of Carbon Nitride, *ACS Omega*, 2019, **4**(4), 6114–6125, DOI: 10.1021/acsomega.9b00179.

60 Y. Xie, Y. Pan and P. Cai, Cellulose-Based Antimicrobial Films Incroporated with ZnO Nanopillars on Surface as Biodegradable and Antimicrobial Packaging, *Food Chem.*, 2022, **368**, 130784, DOI: 10.1016/j.foodchem.2021.130784.

61 M. A. A. El, G. Mahmoud, M. E. Abdelgawad and M. R. Ahmed, Enhancing the RO Performance of Cellulose Acetate Membrane Using Chitosan Nanoparticles, *J. Polym. Res.*, 2020, 1–12, DOI: 10.1007/s10965-020-02319-7.

62 A. Ahmed, M. Bilal, K. Niazi, Z. Jahan, T. Ahmad, A. Hussain, E. Pervaiz, H. Ahmed and Z. Hussain, In-Vitro and in-Vivo Study of Superabsorbent PVA/Starch/g-C3N4/Ag@TiO2 NPs Hydrogel Membranes for Wound Dressing, *Eur. Polym. J.*, 2020, **130**, 109650, DOI: 10.1016/j.eurpolymj.2020.109650.

63 T. Hou, S. Ma, F. Wang and L. Wang, A Comprehensive Review of Intelligent Controlled Release Antimicrobial Packaging in Food Preservation, *Food Sci. Biotechnol.*, 2023, **32**(11), 1459–1478, DOI: 10.1007/s10068-023-01344-8.

64 A. Sharkawy, M. Barreiro and A. Rodrigues, Chitosan-Based Pickering Emulsions and Their Applications: A Review, *Carbohydr. Polym.*, 2020, **250**, 116885, DOI: 10.1016/j.carbpol.2020.116885.

65 R. Olmos-Juste, B. Alonso-Lerma, R. Pérez-Jiménez, N. Gabilondo and A. Eceiza, 3D Printed Alginate-Cellulose Nanofibers Based Patches for Local Curcumin Administration, *Carbohydr. Polym.*, 2021, **264**, 118026, DOI: 10.1016/j.carbpol.2021.118026.

66 I. Al-jaf, B. Akyuz Yilmaz, T. Karaduman Yesildal, L. Akyuz and M. Kaya, Production and Characterization of Chitosan-Based Superhydrophobic Film Bio-Inspired by Verbascum Sp. Leaf, *Int. J. Biol. Macromol.*, 2025, **307**, 142186, DOI: 10.1016/j.ijbiomac.2025.142186.

67 Y. Lin, Y. Tian, H. Sun and T. Hagio, Progress in Modifications of 3D Graphene-Based Adsorbents for Environmental Applications, *Chemosphere*, 2021, **270**, 129420, DOI: 10.1016/j.chemosphere.2020.129420.

68 M. S. Hossain, B. Adak, Khushbu and S. Mukhopadhyay, Graphitic Carbon Nitride-Reinforced Chitosan/Ca2+-Alginate Nanocomposite Films with Multifunctional Properties for Sustainable Packaging, *ACS Appl. Bio Mater.*, 2025, **8**(10), 9123–9139, DOI: 10.1021/acsabm.5c01293.

69 A. Ahmed, B. Adak, T. Bansala and S. Mukhopadhyay, Green Solvent Processed Cellulose/Graphene Oxide Nanocomposite Films with Superior Mechanical, Thermal, and Ultraviolet Shielding Properties, *ACS Appl. Mater. Interfaces*, 2020, **12**(1), 1687–1697, DOI: 10.1021/acsami.9b19686.

70 Y. Shi, Z. Gui, B. Yu, R. K. K. Yuen, B. Wang and Y. Hu, Graphite-like Carbon Nitride and Functionalized Layered Double Hydroxide Filled Polypropylene-Grafted Maleic Anhydride Nanocomposites: Comparison in Flame Retardancy, and Thermal, Mechanical and UV-Shielding Properties, *Composites, Part B*, 2015, **79**, 277–284, DOI: 10.1016/j.compositesb.2015.04.046.

71 A. M. Ismail, M. I. Mohammed and I. S. Yahia, A Facile Method to Prepare G-Carbon Nitride/Poly(Vinyl Alcohol) Nanocomposite Films with Remarkable Optoelectrical Properties: Laser Attenuation Approach, *Opt. Laser Technol.*, 2021, **134**, 106600, DOI: 10.1016/j.optlastec.2020.106600.

72 H. Wang, J. Qian and F. Ding, Emerging Chitosan-Based Films for Food Packaging Applications, *J. Agric. Food Chem.*, 2018, **66**(2), 395–413, DOI: 10.1021/acs.jafc.7b04528.

73 M. Zare, K. Namratha, S. Ilyas, A. Hezam, S. Mathur and K. Byrappa, Smart Fortified PHBV-CS Biopolymer with ZnO-Ag Nanocomposites for Enhanced Shelf Life of Food Packaging, *ACS Appl. Mater. Interfaces*, 2019, **11**(51), 48309–48320, DOI: 10.1021/acsami.9b15724.

74 O. A. Silva, M. C. G. Pellá, J. C. C. Friedrich, M. G. Pellá, A. G. Beneton, M. G. I. Faria, G. A. L. Colauto, J. Caetano, M. R. Simões and D. C. Dragunski, Effects of a Native Cassava Starch, Chitosan, and Gelatin-Based Edible Coating over Guavas (Psidium Guajava L.), *ACS Food Sci. Technol.*, 2021, **1**(7), 1247–1253, DOI: 10.1021/acsfoodscitech.1c00131.

75 C. Nunes, M. A. Coimbra and P. Ferreira, Tailoring Functional Chitosan-Based Composites for Food Applications, *Chem. Rec.*, 2018, **18**(7), 1138–1149, DOI: 10.1002/tcr.201700112.

76 K. Mondal, S. K. Bhattacharjee, C. Mudenur, T. Ghosh, V. V. Goud and V. Katiyar, Development of Antioxidant-Rich Edible Active Films and Coatings Incorporated with de-Oiled Ethanolic Green Algae Extract: A Candidate for Prolonging the Shelf Life of Fresh Produce, *RSC Adv.*, 2022, **12**(21), 13295–13313, DOI: 10.1039/d2ra00949h.

77 J. Dong, Y. Zhao, H. Chen, L. Liu, W. Zhang, B. Sun, M. Yang, Y. Wang and L. Dong, Fabrication of PEGylated Graphitic Carbon Nitride Quantum Dots as Traceable, PH-Sensitive Drug Delivery Systems, *New J. Chem.*, 2018, **42**(17), 14263–14270, DOI: 10.1039/c8nj02542h.

78 G. M. Estrada-Villegas, G. Morselli, M. J. A. Oliveira, G. González-Pérez and A. B. Lugão, PVGA/Alginate-AgNPs Hydrogel as Absorbent Biomaterial and Its Soil Biodegradation Behavior, *Polym. Bull.*, 2020, **77**(8), 4147–4166, DOI: 10.1007/s00289-019-02966-x.

79 Y. N. Phang, S. Y. Chee, C. O. Lee and Y. L. Teh, Thermal and Microbial Degradation of Alginate-Based Superabsorbent Polymer, *Polym. Degrad. Stab.*, 2011, **96**(9), 1653–1661, DOI: 10.1016/j.polymdegradstab.2011.06.010.

80 E. G. Arafa, M. W. Sabaa, R. R. Mohamed, E. M. Kamel, A. M. Elzanaty, A. M. Mahmoud and O. F. Abdel-Gawad, Eco-Friendly and Biodegradable Sodium Alginate/Quaternized Chitosan Hydrogel for Controlled Release of Urea and Its Antimicrobial Activity, *Carbohydr. Polym.*, 2022, **291**, 119555, DOI: 10.1016/j.carbpol.2022.119555.

81 M. Iñiguez-Moreno, J. A. Ragazzo-Sánchez and M. Calderón-Santoyo, An Extensive Review of Natural Polymers Used as Coatings for Postharvest Shelf-Life Extension: Trends and Challenges, *Polymers*, 2021, **13**(19), 3271, DOI: 10.3390/polym13193271.

82 I. B. Basumatary, A. Mukherjee, V. Katiyar and S. Kumar, Biopolymer-Based Nanocomposite Films and Coatings: Recent Advances in Shelf-Life Improvement of Fruits and Vegetables, *Crit. Rev. Food Sci. Nutr.*, 2022, **62**(7), 1912–1935, DOI: 10.1080/10408398.2020.1848789.

83 Y. Li, S. Rokayya, F. Jia, X. Nie, J. Xu, A. Elhakem, M. Almatrafi, N. Benajiba and M. Helal, Shelf-Life, Quality, Safety Evaluations of Blueberry Fruits Coated with Chitosan Nano-Material Films, *Sci. Rep.*, 2021, **11**(1), 55, DOI: 10.1038/s41598-020-80056-z.

84 D. Pratap Singh and G. Packirisamy, Biopolymer Based Edible Coating for Enhancing the Shelf Life of Horticulture Products, *Food Chem.:Mol. Sci.*, 2022, **4**, 100085, DOI: 10.1016/j.fochms.2022.100085.